LETTER

doi:10.1038/nature21034

mTORC1 and muscle regeneration are regulated by the LINC00961-encoded SPAR polypeptide

Akinobu Matsumoto[1], Alessandra Pasut[1]*, Masaki Matsumoto[2]*, Riu Yamashita[3]*, Jacqueline Fung[1], Emanuele Monteleone[1,4], Alan Saghatelian[5], Keiichi I. Nakayama[2], John G. Clohessy[1] & Pier Paolo Pandolfi[1]

Although long non-coding RNAs (lncRNAs) are non-protein-coding transcripts by definition, recent studies have shown that a fraction of putative small open reading frames within lncRNAs are translated[1–3]. However, the biological significance of these hidden polypeptides is still unclear. Here we identify and functionally characterize a novel polypeptide encoded by the lncRNA LINC00961. This polypeptide is conserved between human and mouse, is localized to the late endosome/lysosome and interacts with the lysosomal v-ATPase to negatively regulate mTORC1 activation. This regulation of mTORC1 is specific to activation of mTORC1 by amino acid stimulation, rather than by growth factors. Hence, we termed this polypeptide 'small regulatory polypeptide of amino acid response' (SPAR). We show that the SPAR-encoding lncRNA is highly expressed in a subset of tissues and use CRISPR/Cas9 engineering to develop a SPAR-polypeptide-specific knockout mouse while maintaining expression of the host lncRNA. We find that the SPAR-encoding lncRNA is downregulated in skeletal muscle upon acute injury, and using this *in vivo* model we establish that SPAR downregulation enables efficient activation of mTORC1 and promotes muscle regeneration. Our data provide a mechanism by which mTORC1 activation may be finely regulated in a tissue-specific manner in response to injury, and a paradigm by which lncRNAs encoding small polypeptides can modulate general biological pathways and processes to facilitate tissue-specific requirements, consistent with their restricted and highly regulated expression profile.

Similar to mRNAs, lncRNAs are transcribed by RNA polymerase II, spliced, capped, and polyadenylated[4–6]. However, some lncRNAs may encode 'hidden' polypeptides (ORFs of fewer than 100 amino acids)[1–3], as recently demonstrated in both *Drosophila melanogaster* and *Caenorhabditis elegans*[7–9]. Moreover, two functional mammalian polypeptides encoded by lncRNAs have been reported to modulate the calcium pump SERCA[10,11]. Thus, given the tissue-specific nature of lncRNA expression in mammals[12], we hypothesized that hidden peptides might be used to finely regulate the activity of biological processes and thereby meet the specific needs of a tissue or organ.

We applied a proteomics strategy to identify novel polypeptides encoded by putative lncRNAs. A detailed description and in-depth analysis of this work will be reported elsewhere (A.M. and P.P.P., manuscript in preparation). From this screening we identified a conserved lncRNA, LINC00961, as harbouring a hidden polypeptide of 90 amino acids. LINC00961 is polyadenylated (Extended Data Fig. 1a) and localizes to actively translating ribosomes (Extended Data Fig. 1b, c). Furthermore, we generated a synthetic peptide and carried out tandem mass spectroscopy (MS/MS) analysis to validate the existence of the endogenous peptide (Extended Data Fig. 1d).

Although LINC00961 was undetectable by quantitative PCR (qPCR) in HEK293T cells, HeLa cells demonstrated high levels of expression (Extended Data Fig. 1e), while qPCR of human and mouse tissue demonstrated high levels of expression in lung, heart and skeletal muscle (Extended Data Fig. 1f, g).

Three putative ORFs with an initiating ATG codon and an ORF longer than 30 amino acids in a sense (+) orientation were present in LINC00961 (Fig. 1a). Of these, ORF1 encoded a putative polypeptide of 90 amino acids (Extended Data Fig. 1h). To validate ORF translation, we inserted a C-terminal Flag-tag at the 3′ end of each ORF (Flag knock-in (KI) 1–3), and confirmed the translation of ORF1 but not the other ORFs (Fig. 1b). ORF1 contains two in-frame ATG codons (Extended Data Fig. 1h, i), and ΔATG constructs established that both ATG codons had the capacity to promote the initiation of translation (Fig. 1c). Although initiation from each codon resulted in differential expression (Fig. 1c), RNA levels and polypeptide stability were indistinguishable between polypeptides (Extended Data Fig. 1j–l), suggesting that translational efficiency affects expression.

LINC00961 harbours a conserved transmembrane domain at its N terminus (Fig. 1d) and localizes to membrane fractions, with its C terminus extending into the cytosol (Extended Data Fig. 2a–d and Supplementary Note 1). Immunofluorescence staining for Flag KI1 in both HeLa and PC3 cells showed punctate staining that co-localized mainly with LAMP1 (a marker for late endosomes and lysosomes[13,14]) but not EEA1 (a marker for early endosomes) or catalase (a marker for peroxisomes; Fig. 1e and Extended Data Fig. 2e, f). Furthermore, using chimaeric reporter fusions between the LINC00961 polypeptide and the human CD8 receptor, we established that the ORF1 C-terminal region of the polypeptide was sufficient for lysosomal localization (Extended Data Fig. 2g–j and Supplementary Note 1).

Finally, we generated polyclonal rabbit anti-ORF1 antibodies and confirmed the endogenous expression of this polypeptide (Fig. 1f and Extended Data Fig. 2k) and the localization of the endogenous peptide in membrane fractions (Fig. 1g).

Mass spectrometry analysis was used to identify the protein interactome for Flag KI1 from HEK293T cells and identified four subunits of the v-ATPase complex (ATP6V0A1, ATP6V0A2, ATP6V0D1 and ATP6AP2; Extended Data Table 1 and Supplementary Table 1). Immunoprecipitation studies confirmed that both V0A1 and V0A2 subunits bound to Flag KI1/ΔATG1 (Fig. 2a). We used two independent antibodies generated against ORF1 to demonstrate binding to endogenous V0A1 and V0A2 (Fig. 2b and Extended Data Fig. 2l). Finally, *in vitro* assays with purified recombinant proteins verified that V0A1 and V0A2 interacted directly with ORF1 (Fig. 2c). These results suggested that this polypeptide might have functions related to the v-ATPase proton pump and the lysosome.

We investigated whether the ORF1 polypeptide influenced v-ATPase complex localization or assembly at steady state, but the data suggested that neither was influenced by the LINC00961 polypeptide (Extended

[1]Cancer Research Institute, Beth Israel Deaconess Cancer Center, Department of Medicine and Pathology, Beth Israel Deaconess Medical Center, Harvard Medical School, Boston, Massachusetts 02215, USA. [2]Department of Molecular and Cellular Biology, Medical Institute of Bioregulation, Kyushu University, Fukuoka 812-8582, Japan. [3]Department of BioBank, Tohoku Medical Megabank Organization (ToMMo), Tohoku University, Sendai 980-8573, Japan. [4]Molecular Biotechnology Center and Department of Molecular Biotechnology and Health Sciences, University of Turin, Via Nizza 52, 10126 Turin, Italy. [5]The Clayton Foundation Laboratories for Peptide Biology, Helmsley Center for Genomic Medicine, Salk Institute for Biological Studies, La Jolla, California 92037, USA. *These authors contributed equally to this work.

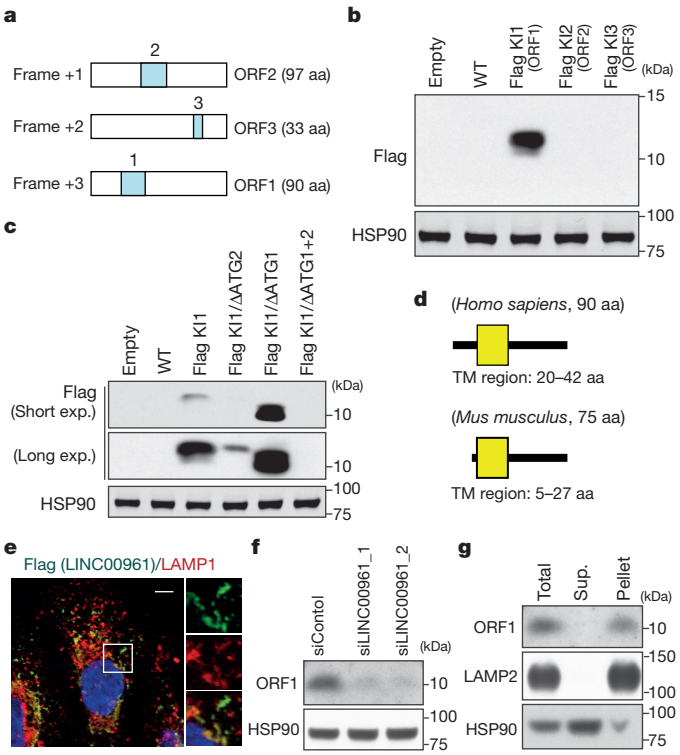

Figure 1 | LINC00961 encodes a novel polypeptide. **a**, Putative ORFs in LINC00961. **b**, **c**, Expression analysis by immunoblotting of Flag KI lncRNAs (**b**) and ΔATG mutants (**c**) in HEK293T cells. WT, wild type. **d**, Putative transmembrane domains predicted by the SMART algorithm. **e**, Representative immunofluorescence images (from $n = 10$ fields of view) of Flag KI1 and LAMP1 in HeLa cells. Scale bar, 5 μm. **f**, **g**, Immunoblotting of lysates (**f**) and fractions (**g**) from HeLa cells for endogenous SPAR.

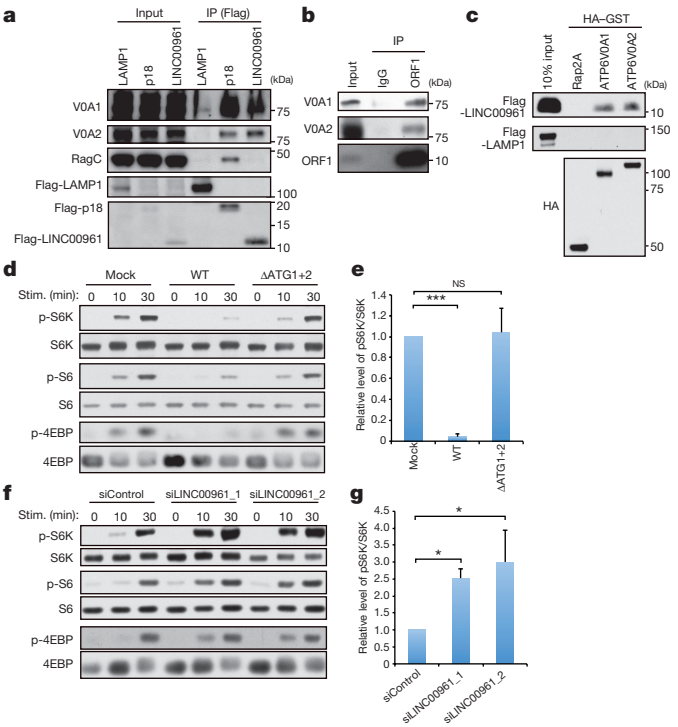

Figure 2 | LINC00961-encoded polypeptide interacts with v-ATPase and regulates mTORC1 signalling in response to amino acids. **a**, **b**, Immunoprecipitation of Flag KI1/ΔATG2 from HEK293T cells (**a**) and endogenous LINC00961-encoded polypeptide from HeLa cells (**b**) followed by immunoblotting. **c**, *In vitro* binding assays using purified Flag KI1/ΔATG2 and GST-ATP6V0A1/V0A2. **d**–**g**, Immunoblotting for phospho-S6K/S6/4EBP from HEK293T cells stably expressing wild-type (WT) LINC00961 or ΔATG1+2 (**d**), and HeLa cells treated with siLINC00961 (**f**) deprived of amino acids for 1 h and stimulated for times shown. Relative levels of phospho-S6K to total S6K at 30 min are quantified in **e** and **g**. Data shown as mean ± s.d. ($n = 3$). $^*P < 0.05$, $^{***}P < 0.001$; one-way ANOVA followed by Tukey's test.

Data Fig. 3a–c and Supplementary Note 2). Similarly, we found no effect of the ORF1 polypeptide on v-ATPase proton pump activity (Extended Data Fig. 3d–k and Supplementary Note 2).

The v-ATPase complex is known to interact with the Ragulator complex at the lysosome to regulate activation of mTORC1 in response to amino acid stimulation[15]. Amino acids activate v-ATPase/Ragulator complexes and Rag GTPases, which promote translocation of mTORC1 to the lysosomal surface, the site of mTORC1 activation[16–18] (Extended Data Fig. 4a). Knockdown or pharmacological inhibition of v-ATPase significantly inhibits mTORC1 activation triggered by stimulation with amino acids[15]. Therefore, we next examined the effects of LINC00961 polypeptide expression on activation of the mTORC1 signalling complex by amino acid stimulation.

HEK293T cells stably overexpressing LINC00961 cDNAs (wild-type LINC00961 or LINC00961(ΔATG1+2)) showed no difference in proliferation (Extended Data Fig. 4b) or steady-state levels of mTORC1 activity as measured by phosphorylation of ribosomal protein S6 kinase (S6K) and the ribosomal protein S6 (S6) (Extended Data Fig. 4c). These HEK293T cell lines were then starved of amino acids for 1 h and stimulated with amino acids for 10 or 30 min. Surprisingly, wild-type LINC00961 strongly inhibited the induction of mTORC1 activity by amino acids (Fig. 2d, e). Importantly, the LINC00961(ΔATG1+2) mutant control failed to alter phosphorylation of S6K, 4EBP or S6 (Fig. 2d, e). Similar results were observed after amino acid starvation in PC3 and HeLa cells (Extended Data Fig. 4d). Furthermore, knocking down LINC00961 in HeLa cells caused increased activation of mTORC1 upon amino acid starvation and stimulation (Fig. 2f, g).

Of the two polypeptides arising from alternative AUG initiation codons in LINC00961, the shorter ΔATG1 polypeptide inhibited mTORC1 activity more potently than the wild-type or ΔATG2 polypeptides (Extended Data Fig. 4e, f), probably owing to increased expression (Fig. 1c). This finding confirms that the 75-amino acid short form of this polypeptide is sufficient to inhibit mTORC1. The Flag-tagged polypeptide (Flag KI1) used to characterize this novel peptide was shown to behave similarly to the wild-type LINC00961 untagged construct (Extended Data Fig. 4g). Furthermore, mislocalization of the LINC00961 polypeptide to mitochondria using two contiguous mitochondrial targeting motifs showed that lysosomal localization was necessary for mTORC1 inhibition (Extended Data Fig. 4h–j).

By contrast, insulin-mediated mTORC1 activation, specific activation mediated by leucine or arginine, and mTORC2 phosphorylation of AKT or ERK1/2 in response to EGF, were not affected by LINC00961 (Extended Data Fig. 5 and Supplementary Note 3). Thus, as the LINC00961-encoded polypeptide appeared to specifically regulate the response to amino acid stimulation, we named this polypeptide 'small regulatory polypeptide of amino acids response' (SPAR).

We investigated whether SPAR expression altered the ability of mTOR to localize to the lysosome in response to amino acid stimulation. Localization of mTOR in conditions of amino acid starvation was predominantly cytoplasmic, with little co-localization with the lysosomal marker LAMP2 (Fig. 3a, b). Amino acid stimulation caused mTOR to correctly re-localize to the lysosome in control cells (Mock), but SPAR-overexpressing cells failed to efficiently re-localize mTOR to the lysosome (WT) (Fig. 3a, b), suggesting that SPAR can impair recruitment of mTORC1 to the lysosome.

Notably, constitutively active Rag expression reversed the inhibition of mTORC1 signalling by SPAR overexpression (Fig. 3c, d). Furthermore, treatment with the v-ATPase inhibitor concanamycin A

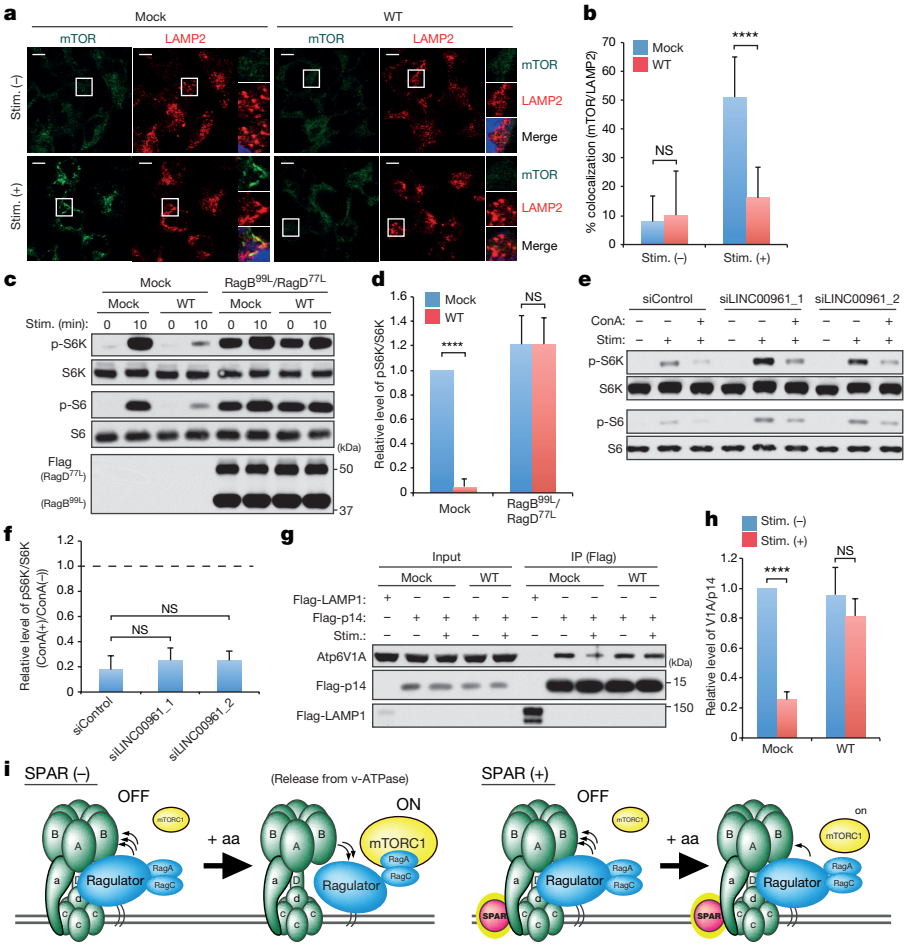

Figure 3 | SPAR promotes interaction of v-ATPase–Ragulator supercomplex to inhibit mTORC1 lysosomal recruitment. **a**, **b**, Representative immunofluorescence images (from 12 fields of view per condition) from HEK293T cells stably expressing wild-type (WT) LINC00961, deprived of amino acids for 1 h and stimulated for 10 min (**a**); co-localization of mTOR with LAMP1 is quantified in **b** ($n = 257$, Mock (−); $n = 288$, WT (−); $n = 271$, Mock (+); $n = 282$, WT (+)). Scale bar, 5 μm. **c**, Phosphorylation of S6K1 and S6 in Mock or RagB^{99L}/RagD^{77L} mutant-expressing HEK293T cells in the presence or absence of wild-type LINC00961. Amino acid treatments carried out as before. **d**, Phospho-S6K/total S6K post-stimulation quantification of results shown in **c** ($n = 3$). **e**, **f**, Phosphorylation of S6K1 and S6 in HeLa cells treated with siLINC00961, deprived of amino acids for 1 h in the presence of concanamycin A (ConA) and subsequently stimulated with amino acids (**e**), with phospho-S6K and total S6K after amino acid stimulation quantified in **f** ($n = 3$). **g**, **h**, Immunoprecipitation of Flag–LAMP1 or Flag–p14 in HEK293T cells stably expressing LINC00961, amino acid starved for 90 min and stimulated for 10 min (**g**), quantified in **h** ($n = 3$). **i**, Model illustrating the mechanistic role of SPAR. Data shown as mean ± s.d., ****$P < 0.0001$; one-way (**f**) or two-way (**b**, **d**, **h**) ANOVA followed by Tukey's test.

(ConA) blocked the increased mTORC1 activity observed upon SPAR knockdown (Fig. 3e, f). These results indicate that SPAR functions upstream of Rags and the Ragulator complex and at the level of the v-ATPase.

Under amino acid starvation conditions, the v-ATPase, Ragulator and Rags exist in a tightly bound supercomplex and mTORC1 cannot associate with the lysosomal surface, so it remains inactive[15,19]. Upon amino acid stimulation, the interactions of this complex are weakened, resulting in recruitment of mTORC1 to the lysosomal surface. To test whether SPAR can regulate this interaction, we carried out immunoprecipitation of Flag-tagged LAMP1 (negative control) or Flag-tagged p14 (a Ragulator subunit) from control or SPAR-overexpressing cells, under amino acid starvation or stimulation. As expected, control cells demonstrated a decreased interaction between Ragulator complex and v-ATPase upon stimulation with amino acids, whereas in SPAR-overexpressing cells the Ragulator and v-ATPase remained tightly bound during both amino acid starvation and stimulation (Fig. 3g, h). These data suggest a model in which a tightly bound v-ATPase–Ragulator–Rags supercomplex is maintained even upon stimulation with amino acids in the presence of SPAR (Fig. 3i).

In contrast to human LINC00961, the mouse homologue 5430416O09Rik harbours a single initiation AUG codon and shares 65% amino acid identity with the human polypeptide (Extended Data Fig. 6a, b). Expression from this single AUG was confirmed by the use of a ΔATG construct (Extended Data Fig. 6c). Overexpression of the mouse lncRNA in human HEK293T and mouse myoblast C2C12 cells demonstrated functional conservation with human SPAR (Extended Data Fig. 6d, e). Importantly, we also demonstrated the expression of endogenous Spar polypeptide in the mouse skeletal muscle (Extended Data Fig. 6f). Atp6v0a1 and Atp6v0a2 are also expressed in skeletal muscle (Extended Data Fig. 6g, h), and we confirmed that endogenous Spar binds to Atp6v0a1 in skeletal muscle *in vivo* (Extended Data Fig. 6i).

To determine the functional relevance of SPAR *in vivo*, we next generated Spar-deficient mice by CRISPR/Cas9 engineering (Extended Data Fig. 7a–c). We introduced a ΔATG mutation in a C57BL/6J zygote to ablate the polypeptide expression (Fig. 4a) while maintaining the integrity of the host lncRNA (Extended Data Fig. 7d). Whole-genome sequencing (WGS) of three independent Spar-knockout mice confirmed that Cas9 had no notable off-target effects (Extended Data Fig. 7e–g, Supplementary Table 2 and Supplementary Note 4).

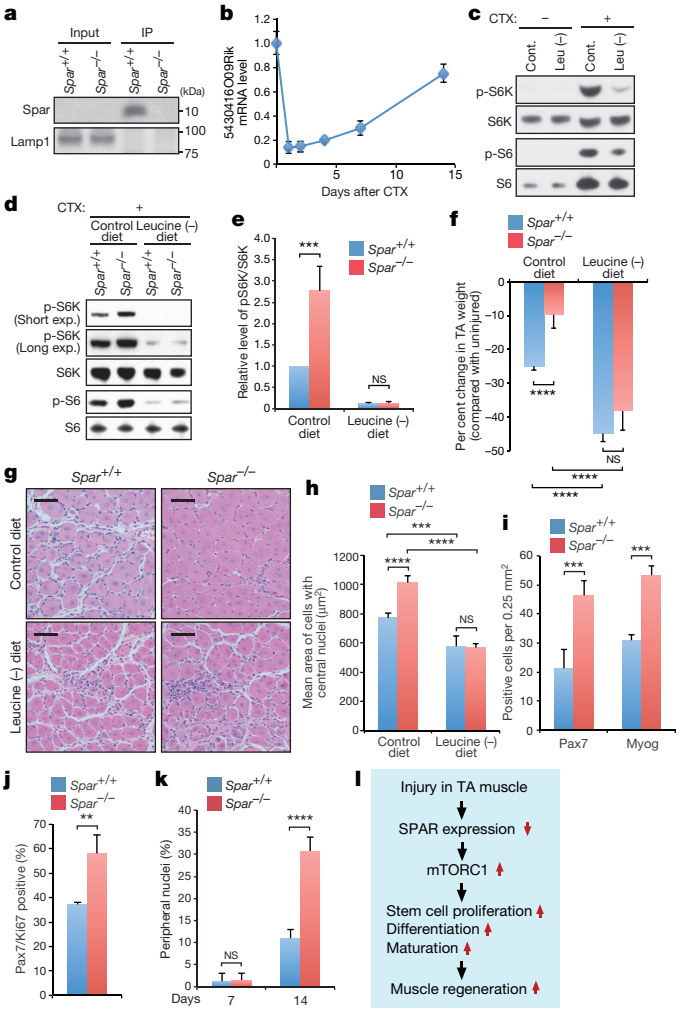

Figure 4 | Loss of Spar promotes muscle regeneration after injury *in vivo*. **a**, Immunoprecipitation of Spar from membrane fractions of skeletal muscle from *Spar*$^{+/+}$ or *Spar*$^{-/-}$ mice followed by immunoblotting. **b**, qRT–PCR for the 5430416O09Rik RNA in tibialis anterior (TA) muscle after CTX injection ($n = 3$). **c**–**e**, Phosphorylation status of S6K1 and S6 in tibialis anterior muscle 4 days after CTX administration (**c**), and from *Spar*$^{+/+}$ and *Spar*$^{-/-}$ mice (**d**) in the setting of control or leucine-free diet; the relative ratio of phospho-S6K to total S6K is quantified in **e** ($n = 3$). **f**–**h**, Per cent change in weight of regenerating tibialis anterior muscle 7 days after CTX administration compared with that of uninjured lateral muscle (**f**). Haematoxylin and eosin staining of CTX-treated tibialis anterior muscle. Representative images from at least ten fields of view per mouse (**g**), and mean area of regenerating cells with central nuclei (**h**). $n = 5$, control diet; $n = 3$, leucine-free diet. Scale bar, 50 μm. **i**, **j**, Number of Pax7-positive cells and myogenin (Myog)-positive cells (**i**) and percentage of cells with Pax7 and Ki67 double-staining (**j**) in tibialis anterior muscle 4 days after injury ($n = 3$). **k**, Percentage of mature cells with peripheral nuclei in tibialis anterior muscle at indicated days after injury ($n = 3$). **l**, Model for the role of SPAR in muscle regeneration. Data shown as mean ± s.d. $^{**}P < 0.01$, $^{***}P < 0.001$, $^{****}P < 0.0001$; *t*-test (**j**) or two-way ANOVA followed by Tukey's test (**e**, **f**, **h**, **i**, **k**).

Spar mutant mice were born at expected Mendelian ratios (Extended Data Fig. 7h) with no gross abnormalities and their body weight was normal up to 8 weeks of age (Extended Data Fig. 7i). As observed in cell cultures *in vitro*, the localization, assembly and lysosomal function of v-ATPase remained intact in both myoblasts and myofibres from *Spar*$^{-/-}$ mice at steady state (Extended Data Fig. 7j–p). As the host lncRNA is highly expressed in skeletal muscle (Extended Data Fig. 1f, g), and mTORC1 signalling is highly activated during regeneration of this tissue[20–23], we hypothesized that Spar may be an important regulator of mTORC1 activity in this setting. Consistent with this hypothesis, treatment with the mTORC1 inhibitor rapamycin greatly inhibited muscle regeneration and confirmed the relevance of mTORC1 in this process (Extended Data Fig. 8a–g and Supplementary Note 5). Cardiotoxin (CTX) is a snake toxin that induces muscle injury and is used in the study of muscle regeneration. Administration of CTX induced a marked, acute reduction in the expression of 5430416O09Rik in wild-type tibialis anterior muscle compared to control lateral uninjured muscle, with expression steadily normalizing during the two-week regeneration period (Fig. 4b). As expected, the stem cell marker Pax7 and the early differentiation marker myogenin peaked early during regeneration (Extended Data Fig. 8h). Together, these data lead us to hypothesize that Spar expression may negatively impact the ability of mTORC1 to promote regeneration after acute injury.

We therefore inhibited mTORC1 using leucine deficiency, as leucine deficiency negates mTORC1 activation at the level of Rags and activates sestrin 1/2, inhibiting mTORC1 activation independent of the SPAR/v-ATPase pathway (Extended Data Fig. 4a). This inhibition was confirmed *in vivo* in tibialis anterior muscle, as shown by blotting for phosphorylation of S6K and S6 after CTX administration (Fig. 4c). Consistent with our *in vitro* data, tibialis anterior muscle from *Spar*$^{-/-}$ mice showed increased phosphorylation of S6K and S6, highlighting hyperactivation of mTORC1 in the absence of Spar, whereas inactivation of mTORC1 signalling by leucine deprivation blocked this activation in tibialis anterior muscle from both *Spar*$^{+/+}$ and *Spar*$^{-/-}$ mice (Fig. 4d, e and Extended Data Fig. 8i). As hypothesized, injured *Spar*$^{-/-}$ tibialis anterior muscle demonstrated an increased regenerative capacity (Fig. 4f, Extended Data Fig. 8j–o and Supplementary Note 6). Importantly, mice deprived of leucine failed to efficiently regenerate muscle (Fig. 4f), confirming the role of mTORC1 and Spar in this process.

Regenerating muscles are characterized by myofibres with centrally located nuclei. The number of regenerating myofibres was substantially increased in Spar-deficient tibialis anterior muscle (Fig. 4g, h and Extended Data Fig. 9a, b). Spar-deficient myofibres were also larger, consistent with the role and function of mTORC1, and this increase in size was negated by leucine deprivation (Extended Data Fig. 9c, d). By contrast, we found no significant differences in myofibre size in uninjured tibialis anterior muscles between *Spar*$^{+/+}$ and *Spar*$^{-/-}$ mice (Extended Data Fig. 9e, f). Furthermore, immunostaining and western blot analyses confirmed that Spar-deficient tibialis anterior muscles contained increased numbers of Pax7-positive and Myog-positive cells (Fig. 4i and Extended Data Fig. 9g–k). Similarly, the percentage of Pax7/Ki67 double-positive cells was upregulated (Fig. 4j and Extended Data Fig. 9l), indicating that stem cells have an increased proliferation capacity in Spar-deficient tibialis anterior muscle.

Finally, we analysed the effect of Spar depletion on the maturation of myofibres during regeneration. Seven days after injury, most myofibres from both *Spar*$^{+/+}$ and *Spar*$^{-/-}$ mice were in a regenerative state (Fig. 4k). However, by 14 days, Spar-deficient tibialis anterior muscles had a substantially increased number of mature cells, as measured by a peripheral nucleus, showing that myofibres matured more rapidly in Spar-deficient tibialis anterior muscle (Fig. 4k and Extended Data Fig. 9m). Thus, Spar inactivation promotes muscle regeneration through increased mTORC1 activation, which in turn promotes stem cell proliferation, differentiation, and myofibre maturation (Fig. 4l). These findings were also confirmed in other muscles including the gastrocnemius (Extended Data Fig. 9n–s).

Together, our results show that SPAR is a functional and conserved lncRNA-encoded polypeptide that regulates mTORC1 activation in mammals. Through our characterization of the role of SPAR, we determine a manner by which mTORC1 activation may be tailored in a cell- and tissue-specific manner, and underscore the multiple layers of mTORC1 regulation required in the fine-tuning of this process. Additionally, and more generally, these data emphasize that lncRNA-encoded polypeptides are more than just translational noise, and can encode functionally relevant polypeptides with clinical and therapeutic relevance.

Online Content Methods, along with any additional Extended Data display items and Source Data, are available in the online version of the paper; references unique to these sections appear only in the online paper.

Received 8 December 2014; accepted 6 December 2016.
Published online 26 December 2016.

1. Ingolia, N. T., Lareau, L. F. & Weissman, J. S. Ribosome profiling of mouse embryonic stem cells reveals the complexity and dynamics of mammalian proteomes. *Cell* **147,** 789–802 (2011).
2. Kim, M. S. *et al.* A draft map of the human proteome. *Nature* **509,** 575–581 (2014).
3. Slavoff, S. A. *et al.* Peptidomic discovery of short open reading frame-encoded peptides in human cells. *Nat. Chem. Biol.* **9,** 59–64 (2013).
4. Birney, E. *et al.* Identification and analysis of functional elements in 1% of the human genome by the ENCODE pilot project. *Nature* **447,** 799–816 (2007).
5. Carninci, P. *et al.* The transcriptional landscape of the mammalian genome. *Science* **309,** 1559–1563 (2005).
6. Derrien, T. *et al.* The GENCODE v7 catalog of human long noncoding RNAs: analysis of their gene structure, evolution, and expression. *Genome Res.* **22,** 1775–1789 (2012).
7. Pauli, A. *et al.* Toddler: an embryonic signal that promotes cell movement via Apelin receptors. *Science* **343,** 1248636 (2014).
8. Kondo, T. *et al.* Small peptides switch the transcriptional activity of Shavenbaby during *Drosophila* embryogenesis. *Science* **329,** 336–339 (2010).
9. Magny, E. G. *et al.* Conserved regulation of cardiac calcium uptake by peptides encoded in small open reading frames. *Science* **341,** 1116–1120 (2013).
10. Anderson, D. M. *et al.* A micropeptide encoded by a putative long noncoding RNA regulates muscle performance. *Cell* **160,** 595–606 (2015).
11. Nelson, B. R. *et al.* A peptide encoded by a transcript annotated as long noncoding RNA enhances SERCA activity in muscle. *Science* **351,** 271–275 (2016).
12. Cabili, M. N. *et al.* Integrative annotation of human large intergenic noncoding RNAs reveals global properties and specific subclasses. *Genes Dev.* **25,** 1915–1927 (2011).
13. Humphries, W. H., IV, Szymanski, C. J. & Payne, C. K. Endo-lysosomal vesicles positive for Rab7 and LAMP1 are terminal vesicles for the transport of dextran. *PLoS One* **6,** e26626 (2011).
14. Rebsamen, M. *et al.* SLC38A9 is a component of the lysosomal amino acid sensing machinery that controls mTORC1. *Nature* **519,** 477–481 (2015).
15. Zoncu, R. *et al.* mTORC1 senses lysosomal amino acids through an inside-out mechanism that requires the vacuolar H^+-ATPase. *Science* **334,** 678–683 (2011).
16. Bar-Peled, L. & Sabatini, D. M. Regulation of mTORC1 by amino acids. *Trends Cell Biol.* **24,** 400–406 (2014).
17. Sancak, Y. *et al.* Ragulator-Rag complex targets mTORC1 to the lysosomal surface and is necessary for its activation by amino acids. *Cell* **141,** 290–303 (2010).
18. Sancak, Y. *et al.* The Rag GTPases bind raptor and mediate amino acid signaling to mTORC1. *Science* **320,** 1496–1501 (2008).
19. Bar-Peled, L., Schweitzer, L. D., Zoncu, R. & Sabatini, D. M. Ragulator is a GEF for the rag GTPases that signal amino acid levels to mTORC1. *Cell* **150,** 1196–1208 (2012).
20. Bentzinger, C. F. *et al.* Skeletal muscle-specific ablation of raptor, but not of rictor, causes metabolic changes and results in muscle dystrophy. *Cell Metab.* **8,** 411–424 (2008).
21. Ge, Y. *et al.* mTOR regulates skeletal muscle regeneration *in vivo* through kinase-dependent and kinase-independent mechanisms. *Am. J. Physiol. Cell Physiol.* **297,** C1434–C1444 (2009).
22. Pereira, M. G. *et al.* Leucine supplementation accelerates connective tissue repair of injured tibialis anterior muscle. *Nutrients* **6,** 3981–4001 (2014).
23. Zhang, P. *et al.* mTOR is necessary for proper satellite cell activity and skeletal muscle regeneration. *Biochem. Biophys. Res. Commun.* **463,** 102–108 (2015).

Supplementary Information is available in the online version of the paper.

Acknowledgements We thank members of the P.P.P. laboratory, C. C. Dibble for critical discussions and Cell Signaling Technology for generation of SPAR antibodies. A.M. was supported by a postdoctoral fellowship from JSPS, The Uehara Memorial Foundation and The Naito Foundation. This work was supported in part by NIH grant R01 CA082328 and R35 CA197529 to P.P.P. and JST and PREST to A.M.

Author Contributions A.M. conceived the project, designed and performed most experiments, interpreted the results, and co-wrote the manuscript. A.P. performed muscle experiments. M.M. performed mass spectrometry. R.Y. performed informatic analysis. J.F. performed histology and immunoblotting experiments. E.M. analysed whole-genome sequencing data. A.S. and K.I.N. supervised experimental designs. J.G.C. supervised experimental designs and co-wrote the manuscript. P.P.P. conceived the project, supervised experimental designs, interpreted results, and co-wrote the manuscript.

Author Information Reprints and permissions information is available at www.nature.com/reprints. The authors declare no competing financial interests. Readers are welcome to comment on the online version of the paper. Correspondence and requests for materials should be addressed to P.P.P. (ppandolf@bidmc.harvard.edu).

Reviewer Information *Nature* thanks K.-L. Guan, M. Rüegg and the other anonymous reviewer(s) for their contribution to the peer review of this work.

METHODS

Cell lines and antibodies. All cell lines were obtained from ATCC and checked for mycoplasma by MycoAlert Mycoplasma Detection Kit (Lonza). The following primary antibodies were used: p70 S6K (49D7) (#2708), phospho-p70 S6K (T389, 108D2) (#9234), S6 ribosomal protein (5G10) (#2217), phospho-S6 ribosomal protein (S235/236) (#2211), 4E-BP1 (53H11) (#9644), phospho-4E-BP1 (Ser65) (#9451), p44/42 MAPK (#9102), phospho-p44/42 MAPK (T202/Y204, 20G11) (#4376), Akt (#9272), phospho-Akt (S473) (#9271), RagC (D31G9) (#5466), EEA1 (C45B10) (#3288), catalase (D4P7B) (#12980), GAPDH (C16H11) (#5174), LAMP1 for human (D2D11) (#9091), LAMP1 for mouse for western blotting (C54H11) (#3243) and mTOR (7C10) (#2983) (all Cell Signaling Technology); HSP90 (610419, BD Transduction Laboratories); ATP6V0A1 (H-140) (sc-28801), Calnexin (H-70) (sc-11397) and LAMP2 (H4B4) (sc-18822) (all from Santa Cruz Biotechnologies); ATP6V1A (GTX110815, GeneTex) (A01, Abnova); ATP6V0A2 (GTX111275, GeneTex); ATP6V0D1 (ab202899, abcam); GM130 (610822, BD Biosciences), LAMP1 for mouse for immunohistochemistry (1D4B, abcam); Pax7 (Developmental Studies of Hybridoma Bank), myogenin (F5D, Developmental Studies of Hybridoma Bank), Ki67 (RM-9106-S1, Thermo Fisher Scientific), HA.11 (16B12, Covance), laminin (L9393, Sigma), CD8 (C7423, Sigma); Flag M2 (F1804, Sigma); and β-actin (A5316, Sigma). Rabbit polyclonal antibodies raised against human SPAR were generated at Bethyl Laboratories, Inc. (recognizing both human and mouse SPAR), and in collaboration with Cell Signaling Technology (recognizing only human SPAR).

Polysome fractionation. HeLa cells were seeded at 1.5×10^6 cells per 15-cm dish and cultured overnight to ensure subconfluent cultures for polysome analysis. Cells were then incubated with cycloheximide (Sigma) at a final concentration of 100 μg/ml for 15 min. Plates were then washed with ice-cold PBS containing 100 μg/ml cycloheximide (PBS/CHX), scraped, and collected in ice-cold PBS/CHX. Cells were pelleted by centrifugation and subsequently lysed in polysome lysis buffer (20 mM Tris-HCl (pH 7.4); 5 mM $MgCl_2$; 150 mM NaCl; 1% Triton X-100; 1% deoxycholate; 2.5 mM DTT; 200 U/ml RNasin; 100 μg/ml cycloheximide; EDTA-free protease inhibitor (Roche); α_1-antitrypsin (EMD Biosciences)) and incubated on ice for 10 min. Lysates were centrifuged at 7,500 r.p.m. for 5 min at 4 °C, and the supernatant carefully removed. Lysates were loaded on a 15–50% sucrose gradient containing 100 μg/ml cycloheximide, 0.2 mg/ml heparin, and 1 mM DTT. Gradients were centrifuged at 36,000 r.p.m. for 3 h at 4 °C in a Beckman SW40 rotor and subsequently fractionated using an ISCO-Foxy Jr fraction collector. Polysome profiles were measured using a UA-6 absorbance detector connected to the fraction collector and measuring absorbance at 254 nm.

Reverse transcription and real-time (RT) PCR. Total RNA was extracted with PureLink RNA mini kit (Thermo Fisher Scientific) and human total RNA master panel II were purchased from Clontech and subjected to reverse transcription with RETROscript Reverse Transcription Kit (Thermo Fisher Scientific). Oligo-dT primers were used specifically for the detection of polyadenylated RNAs, otherwise random primers were used in the generation of cDNA. The resulting cDNA was then subjected to RT–PCR analysis with SYBR Select Master Mix (Thermo Fisher Scientific) in a StepOnePlus real-time PCR system (Applied Biosystems). The sequences of the various primers (sense and antisense, respectively) were 5′-CTTTGCTGACCTGCTGGATT-3′ and 5′-TCCCCTGTTGACTGGTCATT-3′ for hypoxanthine phosphoribosyl transferase (HPRT, human), 5′- GCCTAAGATGAGCGCAAGTTG-3′ and 5′-TACTAGGCAGATGGCCACAGG-3′ for HPRT (mouse), 5′-CTGTATTC CCCTCCATCGTG-3′ and 5′-TTCAATGGGGTACTTCAGGG-3′ for β-actin (mouse), 5′-AACCAGGACAGAGGCTGC-3′ and 5′-CTGGAAGACGTGA GCACAGA-3′ for endogenous expression of LINC00961 (human), 5′-CTGCTGC TTCAGCTGTGACT-3′ and 5′-AAGAGAGAAGCTTCCTGGCG-3′ for exogenous expression of LINC00961 (human), 5′-GGGTCACCAGCTCCAGATAC-3′ and 5′-AACGCCTCAGGACTTCAAGA-3′ for 5430416O09Rik (mouse), 5′-TCGG CCAGTCATGTATCAAA-3′ and 5′-ACCAAGACTTGTGAGGCCAT-3′ for circHIPK3 (human), 5′-AGCTTGGGAAGGTCCAATTT-3′ and 5′-CGGAGTTTTCGATCCATTTC-3′ for Atp6v0a1 (mouse), 5′-TCGTC GGTGAGGTAAAGAGG-3′ and 5′-TTCAGGCAGGGGAATATCAG-3′ for Atp6v0a2 (mouse), 5′-GACGACGAGGAAGGAGACAA-3′ and 5′-ACATCT GAGCCCTCATCCAG-3′ for Pax7 (mouse), 5′-CAGTGAATGCAACTCCCA CAG-3′ and 5′-ATGGACGTAAGGGAGTGCAGA-3′ for myogenin (mouse). For RNA analysis from polysome fractions, expression was normalized to RNA contained in fraction 1. For detection of polyadenylation, RNA expression was normalized to the signal obtained from cDNA generated using random primers. For all other experiments, results were normalized to the corresponding amount of HPRT or β-actin mRNA in each sample.

Plasmids. Complementary DNAs were amplified by PCR with primers (for LINC00961: atgcgaattcGGAATCTGTGCTCACGTCTTCC and atgcgatatc TATTCAGGGCTGGATACAGACATAAG; for 5430416O09Rik: atgcgaattc TAACTCTTGAAGTCCTGAGGCG and atgcgatatcCACCCAAAGCATGT CGCTTC. cDNAs including Flag tag sequences and/or ΔATG mutation were subcloned into pcDNA3 (Invitrogen) and pLVX-puro (Clontech Laboratories), and those for ATP6V1A1 and ATP6V0A2 were subcloned into pRK5-HAGST (Addgene). pRK5-Flag-p14 (#42330), pRK5-p18-Flag (#42331), Flag-pLJM1-RagB-99L (#19315), Flag-pLJM1-RagD-77L (#19317) and LAMP1-mRFP-Flag (#34611) were a gift from D. Sabatini (obtained through Addgene). For Mito-SPAR-Flag construct, SPAR-Flag was substituted with R-GECO1 of CMV-R-mito-GECO1. The vector was a gift from R. Campbell (Addgene plasmid #46021). The other constructs were generated by Gibson assembly master kit (New England BioLabs).

LC–MS/MS analysis. SK-OV-3 cells were lysed by boiling in water for 15 min and mixed with SDS-sample buffer. Proteins were fractionated by SDS–PAGE on 12% Bis-Tris acrylamide NuPAGE gels using MES SDS running buffer (Invitrogen). Lower protein bands (lower than 15 kDa) were excised, divided into 3 fractions and subjected to in-gel digestion. The resulting peptides were analysed by QExactive mass spectrometer coupled to a nano-LC (AdvanceLC, Michrom Inc.) via a nano-electrospray source with a column oven set at 37 °C (AMR Inc.). Samples were dissolved in 0.1% TFA and 2% acetonitrile, and injected to pre-column (L-column micro: 0.3 mm inner diameter, 5 mm length, CERI Japan) and separated by an in-house-made 20-cm column (inner diameter 100 μm, 3μ L-column, CERI, Japan) with a linear gradient (5–35% B for 90 min, 35–95% B for 1 min, and 95% B for 10 min, A: 0.1% formic acid, 2% acetonitrile, B: 0.1% formic acid, 90% acetonitrile) at a flow rate of 250 nl/min. The QExactive was operated in data-dependent mode with survey scans acquired at a resolution of 70,000 at m/z 400. Up to the top 10 most abundant ions with charge 2+ or 3+ from the survey scan were selected with an isolation window of 1.6 Thomson and fragmented by higher-energy collision dissociation with normalized collision energies of 27. The maximum ion injection times for the survey scan and the MS/MS scans were 30 ms and 60 ms, respectively. The ion target values for the survey scan and the MS/MS scans were set to 3×10^6 and 2×10^4, respectively. The acquired MS/MS spectra were analysed with the SEQUEST HT algorithm using a database derived from three-frame (forward only) translation (longer than 5 amino acids) of lncRNA sequences. The search was performed with the following parameters: trypsin was selected as enzyme used, allowed number of missed cleavages was set to 2 and carbamidomethylation on Cys were selected as fixed modification. Oxidized methionine and acetylation at NH_2-terminus were searched as variable modifications. Precursor mass tolerances were 10 p.p.m. and tolerance of MS/MS ions was 0.02 Da. Peptides found to be identical to fragments of annotated proteins were eliminated from the candidate pool. False discovery rate was determined by Percolator algorithm in the Proteome Discoverer suite (q value <0.01). We used a cut-off score of >1.0 for Xcorr and between -5.0 and $+5.0$ for delta mass values. To validate the SPAR peptide spectral pattern, we obtained collision-induced dissociation (CID) spectra of synthesized peptides (QEASLFTGPVR) by LC–MS/MS analysis, and compared each with the original spectra acquired from cell lysate.

Immunoaffinty purification–MS analysis. The affinity-purified protein complexes were fractionated by SDS–PAGE (10%) and stained by silver staining. Protein bands were excised and subjected to in-gel digestion. Peptides were dissolved in a solution containing 0.1% trifluoroacetic acid and 2% acetonitrile and analysed using an LTQ Orbitrap Velos Pro mass spectrometer (Thermo Fisher Scientific) coupled with a nanoLC instrument (Advance, Michrom BioResources) and HTC-PAL autosampler (CTC Analytics). Peptide separation was performed with an in-house pulled fused silica capillary (internal diameter, 0.1 mm; length, 15 cm; tip internal diameter, 0.05 mm) packed with a 3-μm C18 L-column (Chemicals Evaluation and Research Institute). The mobile phases consisted of 0.1% formic acid (A) and 100% acetonitrile (B). Peptides were eluted with a gradient of 5–35% B for 30 min at a flow rate of 200 nl/min. CID spectra were acquired automatically in the data-dependent scan mode with the dynamic exclusion option. Full MS spectra were obtained with Orbitrap in the mass/charge (m/z) range of 300–2,000 with a resolution of 30,000 at m/z 400. The six most intense precursor ions (minimum ion count threshold of 1,000) for the full MS spectra were selected for subsequent ion-trap MS/MS analysis with the automated gain control (AGC) mode. The AGC were set to 1.00×10^6 for full MS and 3.00×10^4 for CID MS/MS. The normalized collision energy values were set to 35%. Lock mass function was activated to minimize mass error during analysis. The CID raw spectra were extracted using MSn.exe (Thermo Fisher Scientific) and subjected to database search using the MASCOT algorithm. The peak list was compared with Human International Protein Index version 3.16 database (European Bioinformatics Institute). Trypsin was selected as the enzyme used, the allowed number of missed cleavages was set at 2, and carbamidomethylation on cysteine was selected as the fixed modification. Oxidized methionine and protein NH_2-acetylation were searched as variable modifications. Precursor mass tolerance was 10 p.p.m., and tolerance of MS/MS ions was 0.8 Da. We extracted peptide-spectrum matches

(PSMs) with MASCOT score >20, peptide length >6 amino acids, precursor delta mass <5 p.p.m. and carried out further validation by using an in-house script. We checked PSMs with low MASCOT score (<35) by the following criteria: 1) difference in MASCOT score from second ranked candidate peptides (designated as delta-score) is more than 12 and consecutive b- or y-ion matching is at least seven, or 2) delta-score is more than 12 and the number of three-consecutive matching is more than three. We approved such PSMs as validated peptide identification by passing either criterion. Furthermore proteins with less than three peptide hits were removed to eliminate low confidence protein identification.

Generation of Spar mutant mice. The T7-Cas9 nickase and T7-sgRNA PCR product were gel purified and used as the template for *in vitro* transcription (IVT) using mMESSAGE mMACHINE T7 ULTRA kit (Thermo Fisher Scientific) and MEGAshortscript T7 kit (Thermo Fisher Scientific), respectively. Both the Cas9 nickase mRNA and the sgRNAs were purified using MEGAclear kit (Life Technologies) and eluted in RNase-free water. Cas9 nickase mRNA (30 ng/ml), sgRNAs (15 ng/ml), and ssDNA oligo (100 ng/ml) were mixed and injected into zygotes from the C57BL/6 strain by the BIDMC Transgenic Core. sgRNA sequences and ssDNA oligo sequences are described in Extended Data Fig. 7a, and potential predicted off-target sites were checked for at http://crispr.mit.edu. The resultant mutant mouse was backcrossed with C57BL/6 mice for a minimum of two generations before carrying out experimental procedures. In addition, WGS of three independent mice, backcrossed with the C57BL/6J line for at least four generations, was carried out to ensure that no additional off-target mutations resulting from the Cas9-mediated engineering were present in Spar knockout mice. To detect the Spar mutation, PCR was performed with the primers AM1286 (5′-ctggcttccgtcttagcaac-3′) and AM1287 (5′-attgccaacctcacacaaca-3′), and the resultant PCR product was digested using a SacII restriction enzyme. All mouse experiments had the approval of the BIDMC institutional animal care and use committee (IACUC) (Protocol #082-2014), and were carried out in accordance with the 'Guide for the Care and Use of Laboratory Animals'.

Whole-genome DNA sequencing and read alignment. Genomic DNA from three biological samples was sheared to 350 bp using a Covaris M220 ultrasonicator. Whole-genome sequencing libraries were prepared using the Swift Biosciences 2S PCR-Free DNA library prep reagents according to manufacturer's protocol. Uniquely indexed libraries were pooled in equimolar ratios and sequenced on an Illumina NextSeq500 with paired-end 150 bp reads at the Dana-Farber Cancer Institute Molecular Biology Core Facilities. The average coverage per sample was 10×. Sequencing reads from each sample were aligned to the C57BL/6J reference genome (GRCm38) using BWA and then merged into a single BAM file using Picard tools. To improve SNP and indel calling, the Genome Analysis Toolkit (GATK) 'IndelRealigner' (http://www.broadinstitute.org/gatk/) was used to realign reads near indels from the Mouse Genomes Project (v5). The BAM files were then re-sorted and quality scores were recalibrated using GATK 'Table Recalibration' and PCR duplicates were marked using Picard 'MarkDuplicates'.

Variant Calling. The GATK UnifiedGenotyper variant caller was run, for both SNPs and indels, on the aligned sequence files (BAM files) and mutations were filtered using GATK 'VariantFiltration' by building a Gaussian mixture model. Briefly, the model was determined adaptively based on a set of known variants (true sites or high confidence sites, mgp v5) to find the best parameters for filtering variants.

Muscle regeneration. Eight-week-old male mice were used for all muscle regeneration studies. On the day of injury, mice were placed under general anaesthesia using isoflurane. Injury of skeletal muscle was induced by injection of 50 μl of 10 μM cardiotoxin (CTX) (EMD Millipore, #217504) in the tibialis anterior muscle or gastrocnemius muscle using an insulin syringe. Mice were euthanized and muscles were removed at the indicated days after injection as outlined in the main text. Importantly, injections and euthanasia were carried out at approximately 2 pm, with all mice euthanized at the same time and the muscles immediately dissected and placed on ice within 1 h in order to minimally impact the *in vivo* activation state of mTORC1 due to feeding. For leucine deprivation assays, mice were fed a complete amino acid control diet or a leucine free (−) diet (PhermaServ) starting 1 day before injury. For rapamycin treatment, rapamycin (LC laboratories) was dissolved in 5% PEG400, 5% Tween 80 and 2% ethanol solution, and administered by intraperitoneal injection daily at 2 mg/kg (50–100 μl).

Histology and immunohistochemistry of muscle sections. For haematoxylin and eosin (H&E) staining, tibialis anterior muscles were fixed in 4% paraformaldehyde (Santa Cruz Biotechnologies) and the paraffin-embedded sections were stained with H&E according to a standard procedure. Quantification analyses were performed using ImageJ software. For immunohistochemistry, freshly isolated tibialis anterior muscles were frozen with a mix of equal amounts of 30% sucrose in PBS and OCT compound (Sakura Finetek USA) in isopentane cooled with liquid nitrogen, and then 10-μm sections were prepared. The sections were fixed with 4% paraformaldehyde for 15 min at room temperature and treated with MOM kit (Vector Laboratories) to block endogenous mouse immunoglobulins in the tissue. The resultant sections were incubated for 16 h at 4 °C in primary antibodies diluted in MOM. diluent. Following three 5-min washes in PBS, sections were incubated with secondary antibodies diluted in MOM diluent for 45 min at room temperature in the dark, then incubated with DAPI for 15 min at room temperature in the dark. Following three 5 min washes with PBS, coverslips were mounted in fluorescent mounting medium (Dako) and imaged on a Zeiss LSM510 meta upright confocal microscope.

Primary myoblast isolation and culture. Primary myoblasts were obtained from 6–8-week-old male mice. Hind limb muscles were dissected out and digested to a fine slurry by sequential incubation in 2% collagenase-dispase (20–30 min). To remove undigested tissue, minced tissue was filtered through a 70 μm mesh filter and centrifuged at 2,000 r.p.m. for 5 min. The cell pellet was then resuspended in pre-warmed medium and pre-plated in a 10 cm plastic dish for 2 h to allow fibroblasts to attach. After 2 h, the cell suspension (enriched in slowly attaching muscle cells) was transferred to a new collagen-coated dish. A homogeneous population of muscle cells was obtained by repeating the pre-plating step over the course of two weeks. Primary myoblast cultures were maintained in collagen-coated dishes and cultured in HAM's F10 (Invitrogen) supplemented with 2.5 ng/μl bFGF (Invitrogen), 20% fetal bovine serum, and penicillin and streptomycin.

Immunofluorescence assays. Cells were fixed with 4% paraformaldehyde for 15 min at room temperature. For Mitotoracker staining, cells were cultured with 200 nM Mitotracker for 30 min before fixation. Cells were then washed 3 times with PBS and permeabilized with PBS containing 0.2% Triton X-100 for 10 min at room temperature. Following 1 h blocking in Odyssey blocking buffer (Li-Cor) diluted 1:1 with PBS at room temperature, coverslips were incubated for 16 h at 4 °C in primary antibodies diluted in blocking buffer containing 0.2% Triton X-100. Following three 5-min washes in PBS, coverslips were incubated with secondary antibodies diluted in blocking buffer containing 0.2% Triton X-100 for 45 min at room temperature in the dark, then incubated with DAPI for 15 min at room temperature in the dark. Following three 5-min washes with PBS, coverslips were mounted in Immu-Mount (Thermo Scientific) and imaged on a Zeiss LSM510 meta upright confocal microscope. Quantification analysis was performed using ImageJ software.

Immunoblotting. Protein samples were subjected to SDS–PAGE on 4–12% Bis-Tris acrylamide NuPAGE gels using MOPS or MES SDS running buffer. Membranes were incubated first with primary antibodies and subsequently secondary HRP-tagged antibodies (Amersham), and signals were visualized with ECL or ECL plus (Amersham). Bands were quantified by densitometric analysis using the ImageJ software program.

Subcellular fractionation and v-ATPase localization. The cells were washed in ice-cold PBS and suspended in TNES buffer (50 mM tris, pH 7.4, 150 mM NaCl, 5 mM EDTA, 250 mM sucrose, and EDTA-free protease inhibitors). For HEK293T cells, the cells were homogenized by 30 passages through a 25 G 5/8 needle. For HeLa cells, the cells were homogenized by 30 passages through a 25 G 5/8 needle and further homogenized by Dounce homogenizer. For skeletal muscle, the tissues were minced in TNES buffer and then homogenized by Dounce homogenizer. Nuclei, mitochondria and unbroken cells were removed by centrifugation at 3,000*g* for 10 min. The resultant supernatant was centrifuged at 120,000*g* for 1 h at 4 °C. The supernatant (cytosolic fraction) was collected, and the pellet (membrane fraction) was suspended in an equal volume of TNES buffer or lysis buffer. Sucrose gradient fractionation to determine v-ATPase localization was performed as previously described[24].

Proteinase K digestion. Proteinase K (final concentration, 0.5 mg/ml) was added to the freshly prepared membrane fraction in the absence or presence of 1% Triton X-100 in TNES buffer without EDTA-free protease inhibitors. The mixtures were incubated on ice for 1 h, after which proteolysis was terminated by the addition of PMSF to a final concentration of 1 mM.

Membrane interaction assay. Cells were homogenized in TNES buffer, and the homogenate was centrifuged at 3,000*g* for 5 min at 4 °C. The resulting supernatant was incubated with 0.1 M Na_2CO_3, 0.1 M NaOH, or 1 M NaCl and was then centrifuged at 120,000*g* for 1 h at 4 °C. The supernatant (cytosolic fraction) was collected, and the pellet (membrane fraction) was suspended in an equal volume of TNES buffer. Samples were analysed by SDS–PAGE.

Immunoprecipitation. For the transient expression assays, HEK293T cells were transfected with Flag-tagged proteins and used after 24 h. Cells were either lysed directly or first treated as outlined in the relevant figures. Cells were lysed in ice-cold lysis buffer (0.3% CHAPS, 10 mM β-glycerol phosphate, 10 mM pyrophosphate, 40 mM HEPES (pH 7.4), 2.5 mM $MgCl_2$ and EDTA-free protease inhibitor). The soluble fractions from cell lysates were immunoprecipitated with anti-Flag magnetic beads (Sigma) for 2 h at 4 °C. Immunoprecipitates were washed three times with lysis buffer containing 150 mM NaCl. Immunoprecipitated proteins were eluted by the addition of 0.5 mg/ml Flag peptide (Sigma), and subjected to immunoblotting. For SPAR immunoprecipitation, HeLa cell lysates, or cytosolic

fraction and membrane fractions from skeletal tissues were precleared by incubating with Dynabeads Protein G (Thermo Fisher Scientific) for 1 h at 4 °C, and then immunoprecipitated with anti-SPAR/Dynabeads Protein G complex for 2 h at 4 °C. Immunoprecipitates were washed three times with lysis buffer containing 150 mM NaCl. Immunoprecipitated proteins were eluted by the sample buffer, and subjected to immunoblotting.

***In vitro* binding assay.** HEK293T cells were transfected separately with Flag-tagged proteins or HA-GST-tagged v-ATPase subunits. Twenty-four hours after transfection, cells were lysed in ice-cold lysis buffer (150 mM NaCl, 40 mM HEPES (pH 7.4), 2 mM EGTA, 2.5 mM MgCl2, 1% Triton X-100, and EDTA-free protease inhibitors). Soluble fractions were immunoprecipitated with anti-Flag magnetic beads (Sigma) to isolate Flag-tagged proteins, or immobilized glutathione magnetic beads (Pierce) to isolate GST-tagged v-ATPase subunits, for 2 h at 4 °C. Samples were washed once in lysis buffer, followed by three washes in lysis buffer supplemented with 500 mM NaCl. Samples were then washed once with binding buffer (40 mM HEPES (pH 7.4), 2 mM EGTA, 2.5 mM MgCl2, 0.3% CHAPS). Flag-tagged proteins were eluted from the affinity beads using a competing 0.5 mg/ml Flag peptide diluted in binding buffer for 1 h at 4 °C. For the binding reaction, HA-GST-tagged v-ATPase subunits were incubated with 10 μl of the eluted Flag-proteins (10% of total purified protein) in a total volume of 50 μl supplemented with 1% BSA and 2 mM DTT, for 1.5 h at 4 °C. Samples were then washed three times in binding buffer, eluted in sample buffer, and subjected to immunoblotting.

Amino acid starvation/stimulation, and serum starvation/insulin stimulation. HEK293T cells were seeded in poly-L-lysine (PLL, Sigma)-coated 6-well plates. For insulin or EGF assay, cells in 6-well plates were rinsed once with PBS and incubated in serum-free DMEM for 24 h, and stimulated with 1 μM insulin (Sigma) or 10 ng/ml EGF (Sigma) for the indicated times. For amino acid stimulation assays, cells in 6-well plates were rinsed once with PBS and incubated in amino acid-free RPMI (United States Biological) with 10% dialysed fetal bovine serum (Thermo Fisher Scientific) for the indicated times, and subsequently stimulated with a 50× mixture of amino acids (Sigma) for indicated times. For single amino acid deprivation and stimulation assays, leucine-free or arginine-free RPMI was generated by adding appropriate amino acids (Sigma) to RPMI for SILAC (Thermo Fischer Scientific) with 10% dialysed fetal bovine serum.

siRNAs. Cells were transfected with 20 nM siRNA in medium. Transfection was performed with DharmaFECT 1 (Dharmacon) according to the manufacturer's recommendations. siGENOME siRNA reagents for nontargeting 2 (siControl) was used for negative controls. The sequences of the siRNAs are as follows (5′ to 3′). LINC00961 no. 1: CCUCAGGGAUCCUUGUUAU (Sigma), LINC00961 no. 2: GCUUCUUACUUGCUCCUAA (Sigma).

Flow cytometry. Lysosomal pH was measured with lysosensor DND-189 (Thermo Fisher Scientific) staining by flow cytometry.

Cathepsin assay. Cathepsin K and L activity was monitored with MagicRed Cathepsin Assay Kit (ImmunoChemistry Technologies) according to the manufacturer's recommendations.

Cell proliferation assay. Cell proliferation was monitored with a Cell Proliferation Kit I (MTT) (Roche) according to the manufacturer's recommendations.

Statistical analysis. No specific blinding method or randomization was applied for mouse experiments, and no statistical methods were used to predetermine sample size. Quantitative data were analysed by two-tailed Student's *t*-test and one-way or two-way ANOVA followed by Tukey's post hoc test. All statistical analyses were performed using GraphPad Prism software. $P < 0.05$ was considered statistically significant.

Data availability. WGS data sets have been deposited in The European Nucleotide Archive (ENA) with the accession number PRJEB15315 and are summarized in Supplementary Table 2. Uncropped images for all immunoblot images are provided in Supplementary Information. Source data for protein interactome for SPAR polypeptide is provided in Supplementary Table 1. All other relevant data are available from the corresponding author on reasonable request.

24. Li Chew, C. *et al. In vivo* role of INPP4B in tumor and metastasis suppression through regulation of PI3K-AKT signaling at endosomes. *Cancer Discov.* **5,** 740–751 (2015).

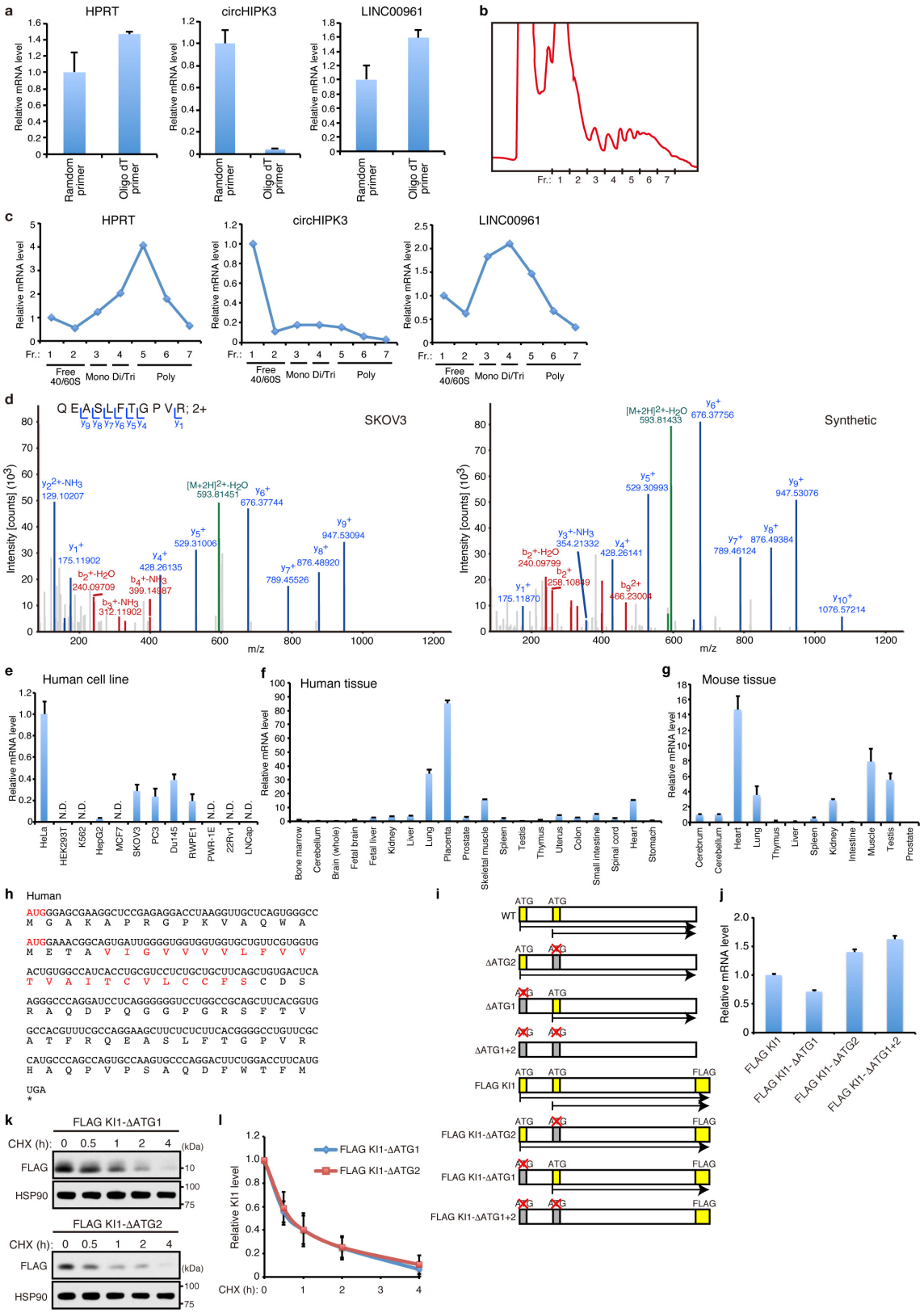

Extended Data Figure 1 | See next page for caption.

Extended Data Figure 1 | Characterization of the LINC00961 RNA and encoded polypeptide. a, qPCR analysis of HPRT, circHIPK3, and LINC00961 using mRNA from HeLa cells reverse transcribed with either random or oligo-dT primers. Data are mean ± s.d. ($n = 3$). **b**, Representative ribosome profile. **c**, HeLa cell lysates were fractionated to collect free 40/60S subunit, monosome, di/trisome and polysome fractions by sucrose gradient centrifugation as shown in **b**. HPRT, circHIPK3, and LINC00961 were extracted from these fractions and quantified by qPCR. **d**, MS/MS spectra from SKOV3 cell lysate of an endogenous polypeptide encoded by LINC00961 (left), and synthetic peptide MS/MS spectra confirming spectral pattern of the endogenous peptide (right). **e**, **f**, qPCR analysis of LINC00961 using RNA isolated from human cell lines (**e**) and human tissues (**f**). Normalized data are expressed relative to the value for HeLa cells and bone marrow, respectively. Data shown as mean ± s.d. of technical triplicates. **g**, qPCR analysis of the mouse homologue 5430416O09Rik in mouse primary tissues. Normalized data are expressed relative to the value for cerebrum. Data shown as mean ± s.d. of technical triplicates. **h**, Nucleotide and amino acid sequences of human LINC00961-encoded polypeptide. AUG codons and transmembrane region are highlighted in red. **i**, Schematic representation of all LINC00961 constructs used in this study. All expression constructs included endogenous 5′ and 3′ UTR regions, but only CDSs are shown here for simplicity. **j**, qPCR analysis of the LINC00961 RNA from HEK293T cells expressing LINC00961 Flag KI1, Flag KI1-ΔATG1, Flag KI1-ΔATG2 and Flag KI1-ΔATG1+2. Normalized data are expressed relative to the value for Flag KI1. Data shown as mean ± s.d. ($n = 3$). **k**, **l**, Cycloheximide (CHX) chase for Flag KI1-ΔATG1 and Flag KI1-ΔATG2 (**d**), quantified in **e**. Data shown as mean ± s.d. ($n = 3$). For gel source images, see Supplementary Fig. 1.

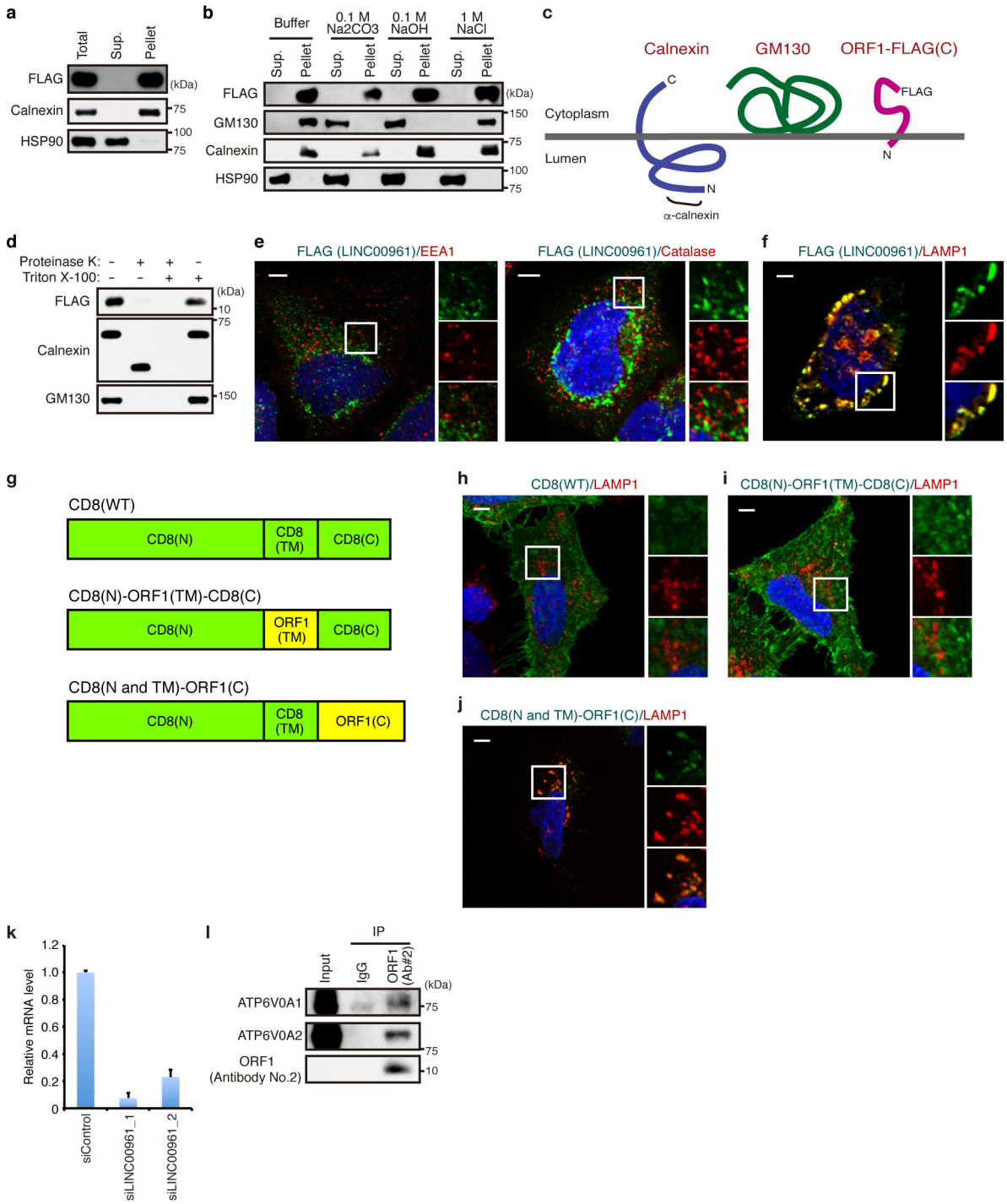

Extended Data Figure 2 | See next page for caption.

Extended Data Figure 2 | Topology and localization of the LINC00961-encoded polypeptide. a, Total, soluble (Sup.) and membrane (Pellet) fractions from HEK293T cells stably expressing Flag KI1 were subjected to immunoblot analysis to evaluate membrane association. **b**, Homogenates of HEK293T cells stably expressing Flag KI1 were incubated with or without 0.1 M Na_2CO_3, 0.1 M NaOH or 1 M NaCl and subsequently centrifuged to yield the soluble fraction (Sup.) and membrane fraction (Pellet). Fractions were then subjected to immunoblot analysis to evaluate membrane integration. **c**, Schematic representation of the membrane topology of calnexin, GM130, and the Flag KI1 LINC00961-encoded polypeptide. The N-terminal epitope of calnexin recognized by the anti-calnexin antibody is indicated. **d**, Membrane fractions from HEK293T cells stably expressing Flag KI1 were incubated in the absence or presence of proteinase K and/or Triton X-100 and were subjected to immunoblot analysis. **e**, Immunofluorescence images for Flag KI1, EEA1 (localized to early endosome) and catalase (localized to peroxisome) in HeLa cells. A representative image from at least three fields of view recorded is shown. Scale bar, 5 μm. **f**, Immunofluorescence images (from two fields of view imaged) demonstrating co-localization of Flag KI1 and LAMP1 in PC3 cells. Scale bar, 2.5 μm. **g**, Schematic representation of chimaeric CD8 and LINC00961-encoded polypeptide (ORF1) fusion constructs used to determine the region responsible for lysosomal localization. **h**–**j**, HeLa cells were transfected with full-length *CD8* (CD8(WT)) (**h**), with a chimaeric CD8 construct with its transmembrane domain replaced with the LINC00961 polypeptide transmembrane domain (CD8(N)-ORF1(TM)-CD8(C)) (**i**), or with a chimaeric construct in which the cytoplasmic region of CD8 was replaced with the LINC00961 polypeptide cytoplasmic region (CD8(N and TM)-ORF1(C)) (**j**). Cells were subsequently subjected to immunofluorescence staining to detect CD8 (Alexa-488) and LAMP1 (Alexa-546). A representative image from at least two fields of view recorded is shown. Scale bar, 5 μm. **k**, qPCR analysis for knockdown of the LINC00961 RNA in HeLa cells treated with siControl, siLINC00961_1 and siLINC00961_2. Normalized data are expressed relative to the value for siControl. Data shown as mean ± s.d. ($n = 3$). **l**, HeLa cell lysates were subjected to immunoprecipitation with IgG control or with antibody no. 2 against LINC00961-encoded polypeptide followed by immunoblotting for ATP6V0A1, ATP6V0A2 and ORF1 using antibody no. 2. For gel source images, see Supplementary Fig. 1.

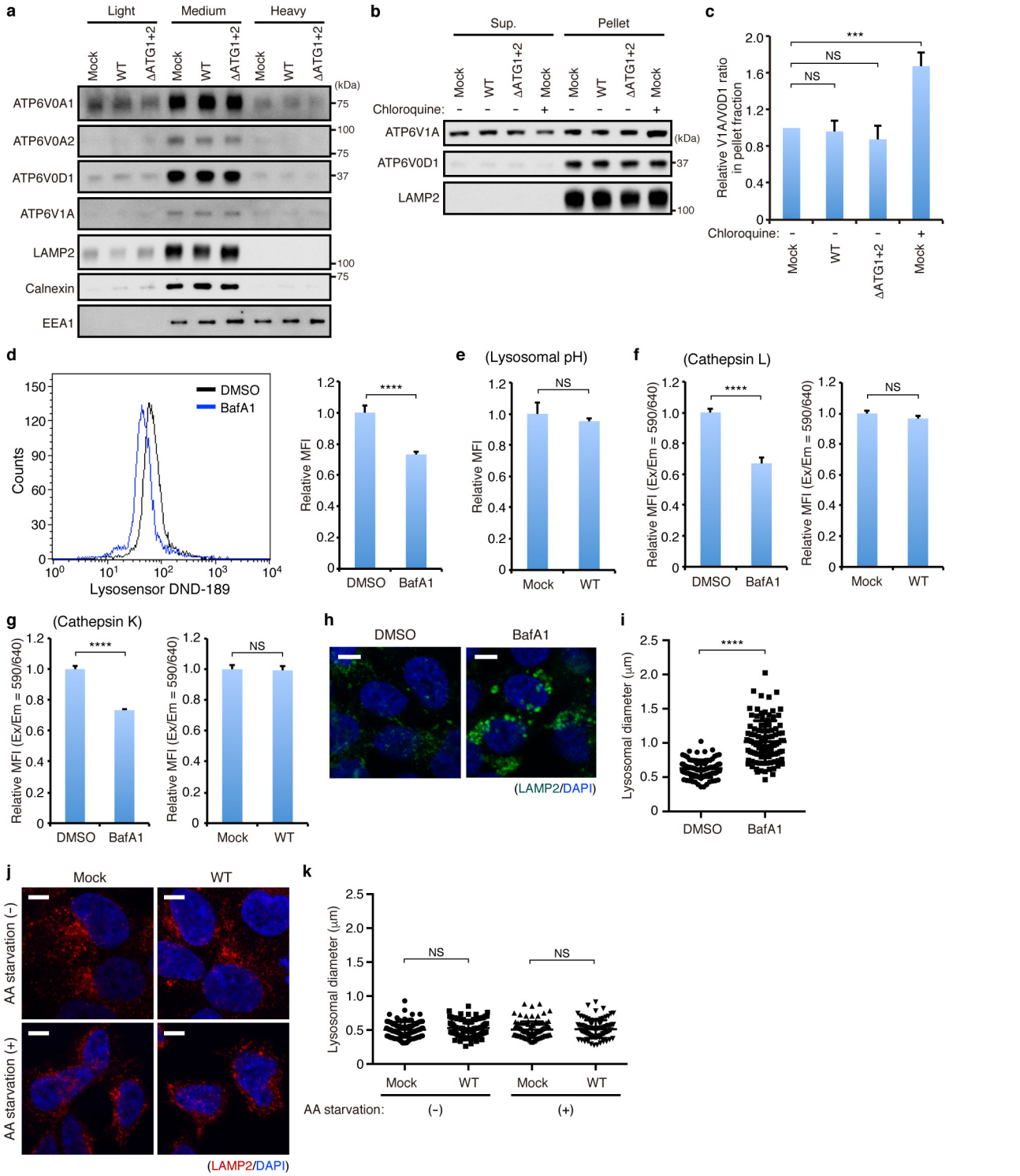

Extended Data Figure 3 | See next page for caption.

Extended Data Figure 3 | v-ATPase localization, assembly and lysosomal functions are unaffected by the LINC00961-encoded polypeptide. a, Localization of v-ATPase subunits was evaluated across membrane fractions by sucrose density gradient fractionation of lysates from HEK293T cells transduced with Mock, wild-type LINC00961 or mutant LINC00961 (ΔATG1+2). v-ATPase localization was characterized by immunoblot analysis for the ATP6V0A1, ATP6V0A2, ATP6V0D1, and ATP6V1A subunits, while immunoblot analysis for LAMP2, calnexin and EEA1 served as controls. **b**, **c**, Soluble (Sup.) and membrane (Pellet) fractions from HEK293T cells stably expressing Mock, wild-type LINC00961 or mutant LINC00961 (ΔATG1+2) were immunoblotted for the V1 domain subunit ATP6V1A, the V0 domain subunit ATP6V0D1, and LAMP2 (**b**). The relative steady-state ratio of ATP6V1A/ATP6V0D1 in pellet fractions was used as a measure of v-ATPase assembly (**c**). Treatment with chloroquine promotes v-ATPase assembly and serves as a positive control to measure changes in assembly. Data shown as mean ± s.d. ($n = 3$). **d**, HEK293T cells were treated for 3 h with DMSO or 200 nM of the v-ATPase inhibitor Bafilomycin A1 (BafA1), an inhibitor of proton pump activity that increases lysosomal pH. Lysosomal pH was monitored by flow cytometry using Lysosensor DND-189 (left), and the mean fluorescence intensity (MFI) plotted to illustrate decreased acidification (right). Data shown as mean ± s.d. ($n = 3$). **e**, HEK293T cells stably expressing empty vector (Mock) or wild-type LINC00961 were used to examine the impact of the LINC00961 polypeptide on lysosomal pH. Cells were analysed by flow cytometry as in **d**, and MFI was plotted. Data are mean ± s.d. ($n = 3$). **f**, **g**, The activity of cathepsin L (**f**) and cathepsin K (**g**) was measured using a Magic Red Cathepsin Assay Kit and quantified. HEK293T cells treated with DMSO or 200 nM BafA1 (positive control) for 3 h (left), or HEK293T cells stably expressing control and wild-type LINC00961 (right), were analysed. Data shown as mean ± s.d. ($n = 3$). **h**–**k**, Lysosomal morphology was analysed by immunostaining for LAMP2. HEK293T cells were treated with DMSO or 20 nM BafA1 for 16 h. A representative image from at least four fields of view recorded is shown (**h**) and lysosomal diameters were measured and quantified (**i**). Similarly, HEK293T cells stably expressing vector control (Mock) or wild-type LINC00961 constructs were analysed with or without amino acid deprivation for 1 h. A representative image from at least six fields of view recorded is shown (**j**) and their lysosomal diameters were measured and quantified (**k**). $n = 100$ loci per condition. Scale bars, 5 μm. $^{***}P < 0.001$, $^{****}P < 0.0001$; Student's *t*-test (**d**–**g**, **i**), or one-way (**c**) or two-way (**k**) ANOVA followed by Tukey's test. For gel source images, see Supplementary Fig. 1.

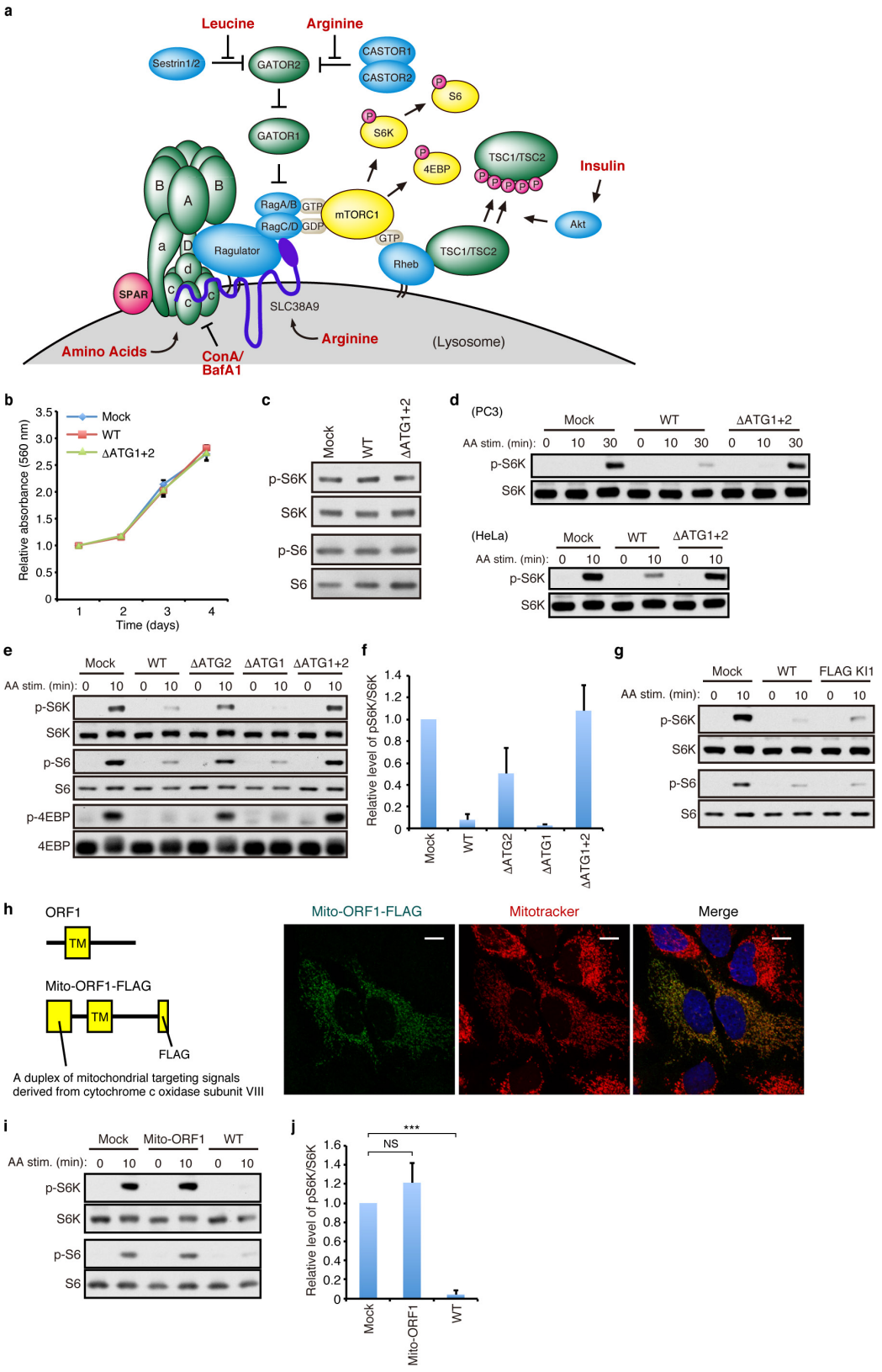

Extended Data Figure 4 | See next page for caption.

Extended Data Figure 4 | mTORC1 regulation by the LINC00961-encoded polypeptide. a, Current model of mTORC1 activation and signalling. This model highlights our current understanding of how mTORC1 is recruited to, and activated at, the lysosome. Rag proteins promote recruitment of mTORC1 to the lysosome where it can be activated by Rheb. Amino acid stimulation releases the Ragulator from the v-ATPase, whereby it interacts with Rags to facilitate mTORC1 recruitment and subsequent activation. Rag proteins can also be regulated through additional mechanisms involving the amino acids leucine and arginine as illustrated. The LINC00961-encoded polypeptide (SPAR) acts at the level of the v-ATPase to promote and stabilize the interaction between the v-ATPase, Ragulator and Rags to inhibit mTORC1 recruitment and activation at the lysosome, even in the presence of amino acid stimulation. **b**, Cell proliferation analysis as analysed by MTT assay in HEK293T cells infected with mock, wild-type LINC00961 and the ΔATG1+2 mutant. Data are mean ± s.d. from technical triplicates. **c**, S6K1 and S6 phosphorylation status remain unchanged in HEK293T cells, stably expressing wild-type LINC00961 and the ΔATG1+2 mutant under steady state conditions. **d**, S6K1 phosphorylation in PC3 (upper panel) and HeLa cells (lower panel) stably expressing wild-type LINC00961 and ΔATG1+2 mutants, deprived of amino acids for 1 h and stimulated with amino acids for indicated times. **e**, **f**, mTORC1 activation as evaluated by S6K1, S6 and 4EBP phosphorylation in HEK293T cells (**e**), and the relative ratio of phospho-S6K to total S6K (**f**), for stably expressing wild-type LINC00961, ΔATG2, ΔATG1 and ΔATG1+2 mutants, deprived of amino acids for 1 h and stimulated with amino acids for 10 min. Data shown as mean ± s.d. ($n = 3$) **g**, mTORC1 activation as evaluated by S6K1 and S6 phosphorylation in HEK293T cells stably expressing wild-type LINC00961 and the Flag KI1 mutant. Cells were deprived of amino acids for 1 h and subsequently stimulated with amino acids for 10 min. **h**, Schematic representation of the LINC00961 ORF1 and Mito-ORF1-Flag, which contains two consecutive mitochondrial targeting signals derived from the cytochrome *c* oxidase subunit VIII fused to the N terminus of LINC00961 ORF1 and a Flag tag at its C terminus (left), and a representative immunofluorescence image, from five fields of view recorded, demonstrating co-localization in HeLa cells of Mito-ORF1-Flag with Mitotracker Red, a marker for mitochondria (right). Scale bar, 10 μm. **i**, **j**, mTORC1 activation as evaluated by S6K1 and S6 phosphorylation in HEK293T cells (**i**), quantified in **j**, for cells stably expressing Mito-ORF1 (without Flag tag) and wild-type LINC00961, deprived of amino acids for 1 h and stimulated for 10 min. Data shown as mean ± s.d. ($n = 3$). $^{***}P < 0.001$. One-way ANOVA followed by Tukey's test (**j**). For gel source images, see Supplementary Fig. 1.

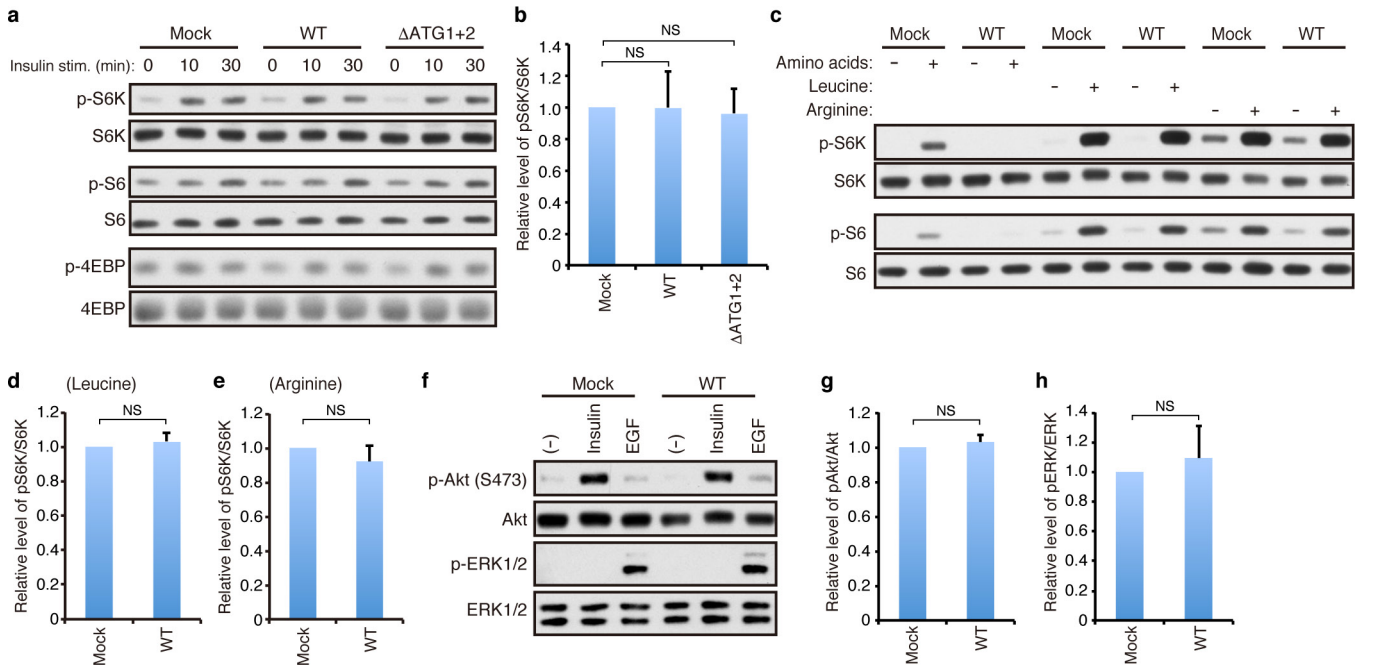

Extended Data Figure 5 | The LINC00961-encoded polypeptide fails to influence signalling independent of amino acid stimulation. **a**, **b**, Phosphorylation status of S6K1, S6 and 4EBP in HEK293T cells stably expressing vector control (Mock), wild-type LINC00961 or mutant LINC00961 (ΔATG1+2), deprived of serum for 24 h and stimulated with 1 μM insulin for the times indicated (**a**), and quantitative analysis of relative level of phospho-S6K to total S6K 30 min after insulin stimulation (**b**). Data shown as mean ± s.d. ($n = 3$). **c**–**e**, S6K1 and S6 and phosphorylation status in HEK293T cells stably expressing vector control (Mock) or wild-type LINC00961 after complete amino acid depletion, leucine depletion or arginine depletion for 1 h and stimulation for 10 min with the respective amino acids as shown (**c**), and quantitative analysis of relative level of phospho-S6K to total S6K after leucine (**d**) or arginine (**e**) stimulation. Data shown as mean ± s.d. ($n = 3$). **f**–**h**, Phosphorylation status of AKT (S473) and ERK1/2 in HEK293T cells stably expressing vector control (Mock) or wild-type LINC00961, deprived of serum for 24 h and stimulated with 1 μM insulin or 10 ng ml^{-1} EGF for 10 min (**f**), and quantitative analysis of relative level of phospho-AKT to total AKT after insulin stimulation (**g**), or phospho-ERK to total ERK after EGF stimulation (**h**). Data shown as mean ± s.d. ($n = 3$). Student's *t*-test (**d**, **e**, **g**, **h**) or one-way ANOVA followed by Tukey's test (**b**). For gel source images, see Supplementary Fig. 1.

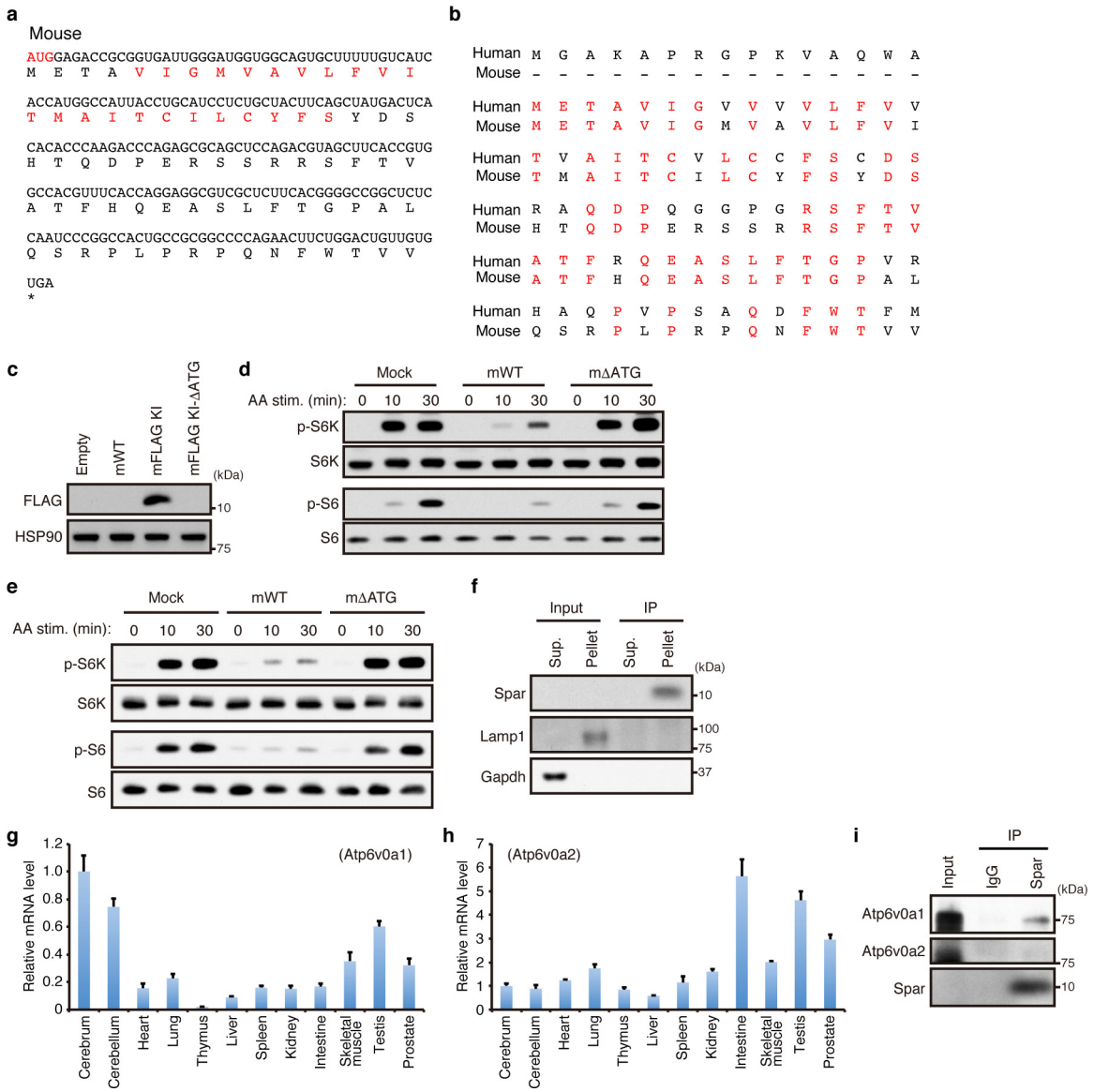

Extended Data Figure 6 | Characterization of mouse Spar. a, Nucleotide and amino acid sequence of the mouse homologue 5430416O09Rik-encoded polypeptide. AUG codon and transmembrane region are highlighted in red. **b**, Polypeptide identity between human and mouse homologues. Identical amino acids are indicated in red. **c**, Immunoblotting with anti-Flag of HEK293T cell lysates transfected with expression constructs for full-length 5430416O09Rik (mWT), C-terminal Flag knockin (mFlag KI), or C-terminal Flag KI with deletion of the initiation ATG (mFlag KI-ΔATG). **d**, **e**, mTORC1 activation as evaluated by S6K1 and S6 phosphorylation in HEK293T cells (**d**) and mouse C2C12 cells (**e**) stably expressing mouse 5430416O09Rik (mWT) or the mΔATG mutant. Cells were deprived of amino acids for 1 h and subsequently stimulated with amino acids for the indicated times. **f**, Membrane (Pellet) and soluble (Sup.) fractions from mouse skeletal muscle were subjected to immunoprecipitation of Spar, followed by immunoblotting for Spar and Lamp1. **g**, **h**, qPCR analysis of mouse Atp6v0a1 (**g**) and Atp6v0a2 (**h**) in mouse primary tissues. Normalized data are expressed relative to the value for cerebrum. Data shown as mean ± s.d. of technical triplicates. **i**, Immunoprecipitation of murine Spar from skeletal muscle lysates followed by immunoblotting for Atp6v0a1 and Atp6v0a2. For gel source images, see Supplementary Fig. 1.

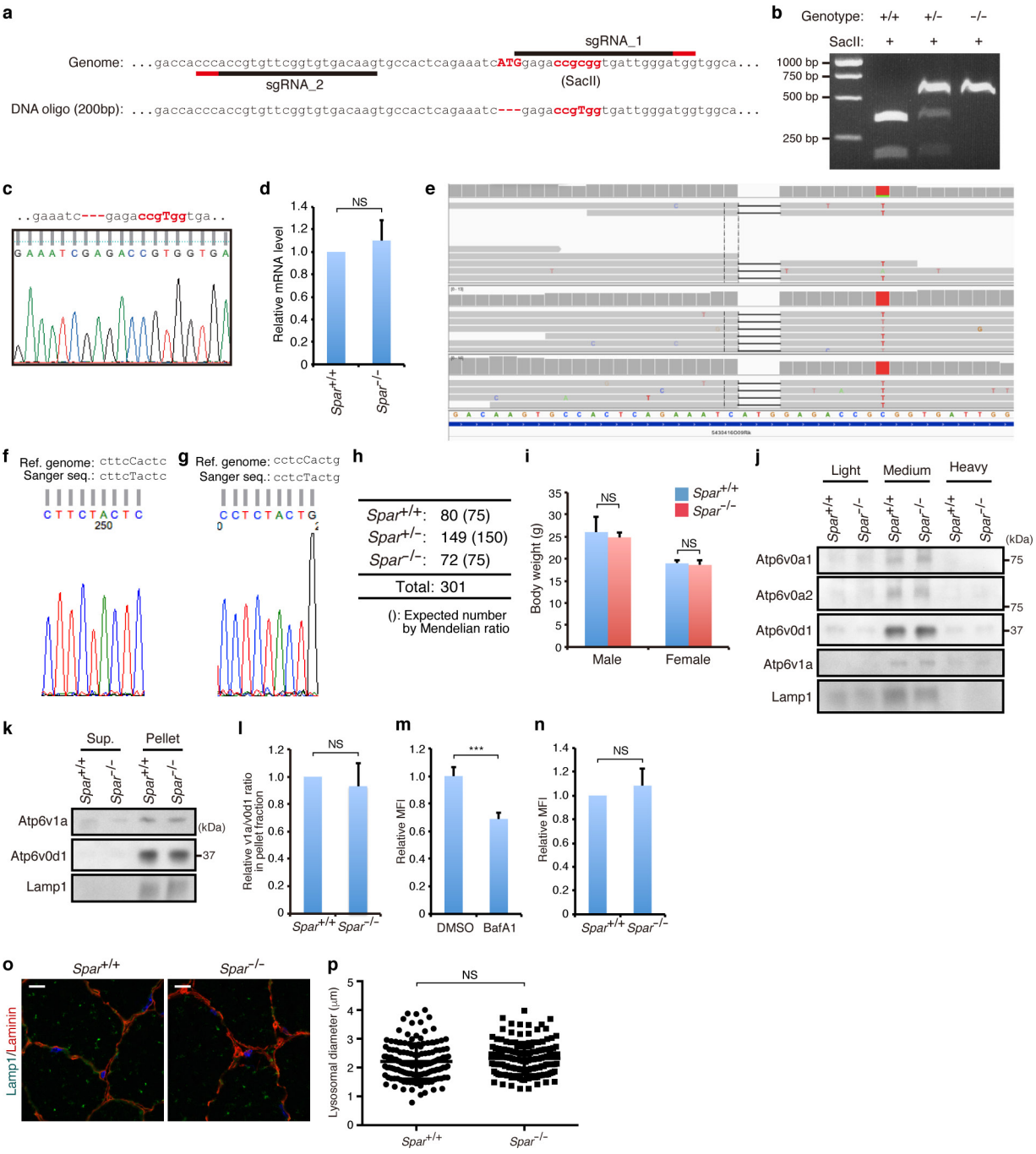

Extended Data Figure 7 | See next page for caption.

Extended Data Figure 7 | Generation and characterization of Spar-deficient mice. a, sgRNA sequences and ssDNA oligo sequence used for CRISPR/Cas9-mediated homologous recombination to generate Spar-deficient mice. ATG initiation codon and SacII restriction enzyme site are highlighted in red. A SacII restriction enzyme site close to the ΔATG was mutated in mutant mice to distinguish the mutant allele from the wild-type allele after PCR. **b**, Analysis of genomic tail DNA by PCR and SacII treatment for mice of the indicated genotypes at 4 weeks of age. **c**, Sanger sequencing result of *Spar* locus from genomic DNA of the $Spar^{-/-}$ mouse. **d**, qRT–PCR analysis of the 5430416O09Rik RNA in tibialis anterior (TA) muscles from $Spar^{+/+}$ and $Spar^{-/-}$ mice. Data shown as mean ± s.d. ($n = 4$). **e**. Confirmation of the Spar mutation by WGS. IGV images show the ΔATG homozygous mutation within the second exon of Spar. **f**, **g**, Sanger sequencing result for SNPs of *Sfi1*-exon5 (**f**) and *Sfi1*-exon13 (**g**) loci from genomic DNA of the $Spar^{-/-}$ mouse. **h**, Frequency of genotypes produced from $Spar^{+/-}$ mouse intercrosses. Numbers in parentheses indicate the expected number by Mendelian ratio. **i**, Bodyweight of $Spar^{+/+}$ and $Spar^{-/-}$ mice at 8 weeks of age. Data shown as mean ± s.d. ($n = 9$). **j**, Localization of v-ATPase subunits in tibialis anterior muscle from $Spar^{+/+}$ and $Spar^{-/-}$ mice was evaluated across membrane fractions by sucrose density gradient fractionation. v-ATPase localization was characterized by immunoblot analysis for the Atp6v0a1, Atp6v0a2, Atp6v0d1, and Atp6v1a subunits, while immunoblot analysis for Lamp1 served as control. **k**, **l**, Soluble (Sup.) and membrane (Pellet) fractions from tibialis anterior muscle of $Spar^{+/+}$ and $Spar^{-/-}$ mice were immunoblotted for the V1 domain subunit Atp6v1a, the V0 domain subunit Atp6v0d1, and Lamp1 (**k**). The relative steady-state ratio of Atp6v1a to Atp6v0d1 in pellet fractions was used as a measure of v-ATPase assembly (**l**). Data shown as mean ± s.d. ($n = 3$). **m**, Myoblasts derived from $Spar^{+/+}$ mice were treated with DMSO or 200 nM of the v-ATPase inhibitor Bafilomycin A1 (BafA1) for 3 h. Lysosomal pH was monitored by flow cytometry using Lysosensor DND-189 and mean fluorescence intensity (MFI) was plotted. Data shown as mean ± s.d. ($n = 3$). **n**, Myoblasts derived from $Spar^{+/+}$ and $Spar^{-/-}$ mice were used to examine the impact of Spar on lysosomal pH. Cells were analysed by flow cytometry as in **m**, and MFI was plotted. Data shown as mean ± s.d. ($n = 3$). **o**, **p**, Lysosomal morphology was analysed by immunostaining for Lamp1 in tibialis anterior muscle from $Spar^{+/+}$ and $Spar^{-/-}$ mice at 8 weeks of age. Representative image (from ten immunofluorescence images recorded per condition) (**o**) and lysosomal diameters were measured and quantified (**p**). $n = 150$ loci per condition. Scale bar, 10 μm. $^{***}P < 0.001$; Student's *t*-test (**d**, **l**–**n**, **p**) or two-way ANOVA followed by Tukey's test (**i**). For gel source images, see Supplementary Fig. 1.

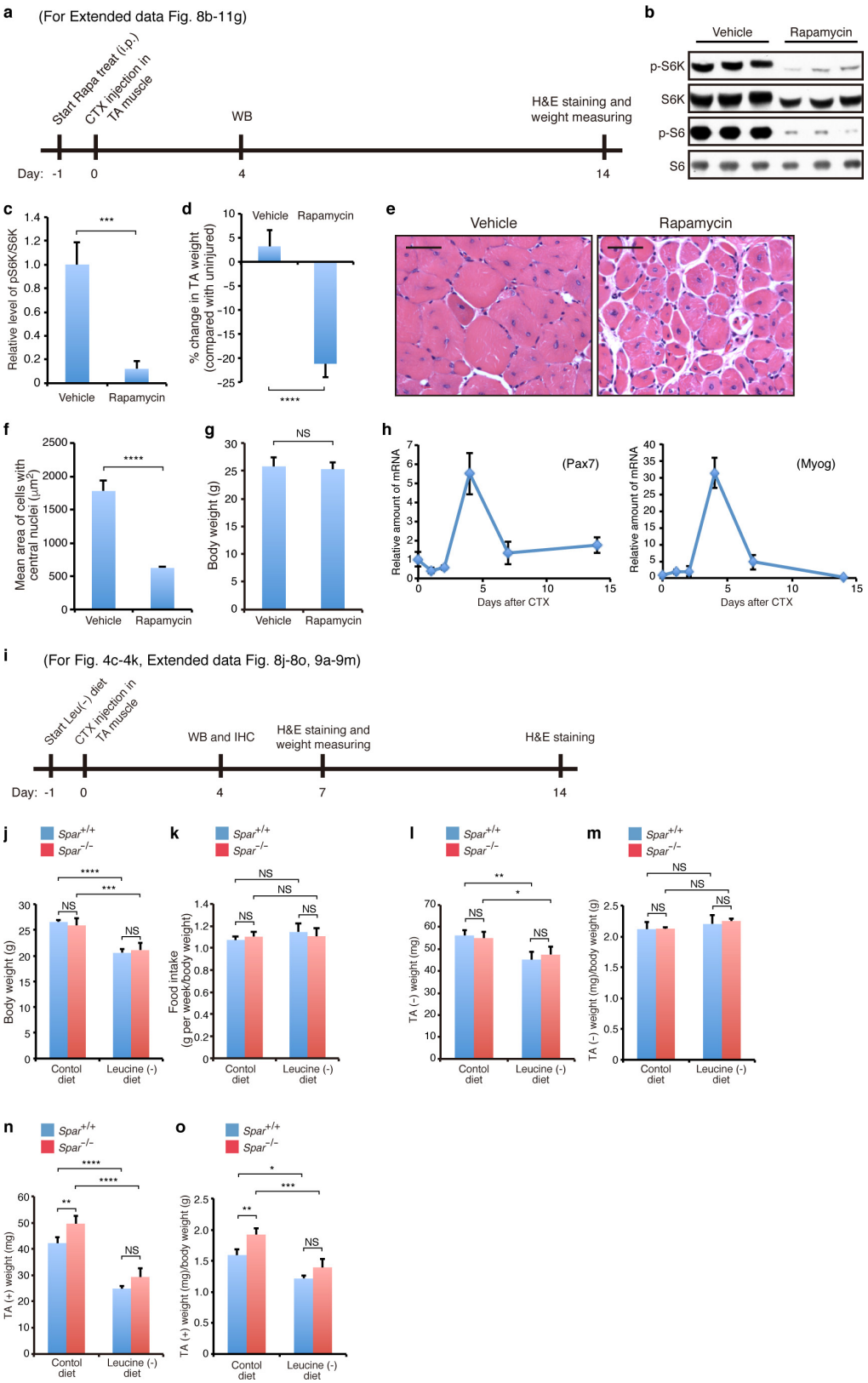

Extended Data Figure 8 | See next page for caption.

Extended Data Figure 8 | Regulation of muscle regeneration by mTORC1 and Spar. a, A schematic outlining the experimental timeline to study the role of mTORC1 in muscle regeneration. Rapamycin (2 mg per kg per day) or vehicle control was administered daily by intraperitoneal (i.p.) injection, with treatment commencing the day before CTX administration. **b**, **c**, S6K1 and S6 phosphorylation status in regenerating tibialis anterior muscle from mice treated with rapamycin or vehicle control 4 days after CTX administration (**b**), and quantitative analysis of relative levels of phospho-S6K to total S6K (**c**). Data shown as mean ± s.d. ($n = 3$). **d**, Per cent change in weight of regenerating tibialis anterior muscle compared with that of uninjured lateral control muscle. Mice were treated with rapamycin or vehicle control one day before CTX administration and muscles analysed 14 days after CTX administration. Data shown as mean ± s.d. ($n = 4$). **e**, **f**, H&E staining of regenerating tibialis anterior muscle from mice treated with vehicle control or rapamycin. Representative images (from at least five fields of view per mouse) (**e**), and quantification of mean area of regenerating cells with central nuclei (**f**). Data shown as mean ± s.d. ($n = 4$). Scale bar, 50 μm. **g**, Bodyweight of mice treated with vehicle control or rapamycin 14 days after CTX administration. Data shown as mean ± s.d. ($n = 4$). **h**, 14-day time course of Pax7 and myogenin expression by qRT–PCR analysis in tibialis anterior muscle from $Spar^{+/+}$ mice post-CTX administration. Data shown as mean ± s.d. ($n = 3$). **i**, A schematic outlining the experimental timeline to study the role of Spar in muscle regeneration. **j**, **k**, Mice were placed on control or leucine-free diet one day before CTX administration, with body weight (**j**) and food intake (**k**) of $Spar^{+/+}$ and $Spar^{-/-}$ mice analysed 7 days after CTX administration. Similar conditions were used in **l**–**o**. **l**, Uninjured lateral control tibialis anterior muscle weight from $Spar^{+/+}$ and $Spar^{-/-}$ mice. **m**, Uninjured lateral control tibialis anterior muscle weights normalized by total body weight in $Spar^{+/+}$ and $Spar^{-/-}$ mice. **n**, Regenerating tibialis anterior muscle weight from $Spar^{+/+}$ and $Spar^{-/-}$ mice. **o**, Regenerating tibialis anterior muscle weights normalized by total body weight from $Spar^{+/+}$ and $Spar^{-/-}$ mice. Data shown as mean ± s.d. ($n = 5$ for control diet, $n = 3$ for leucine-free diet, for **j**, **l**–**o**; $n = 4$ for **k**). $^{*}P < 0.05$, $^{**}P < 0.01$, $^{***}P < 0.001$, $^{****}P < 0.0001$; Student's *t*-test (**c**, **d**, **f**, **g**) or two-way ANOVA followed by Tukey's test (**j**–**o**). For gel source images, see Supplementary Fig. 1.

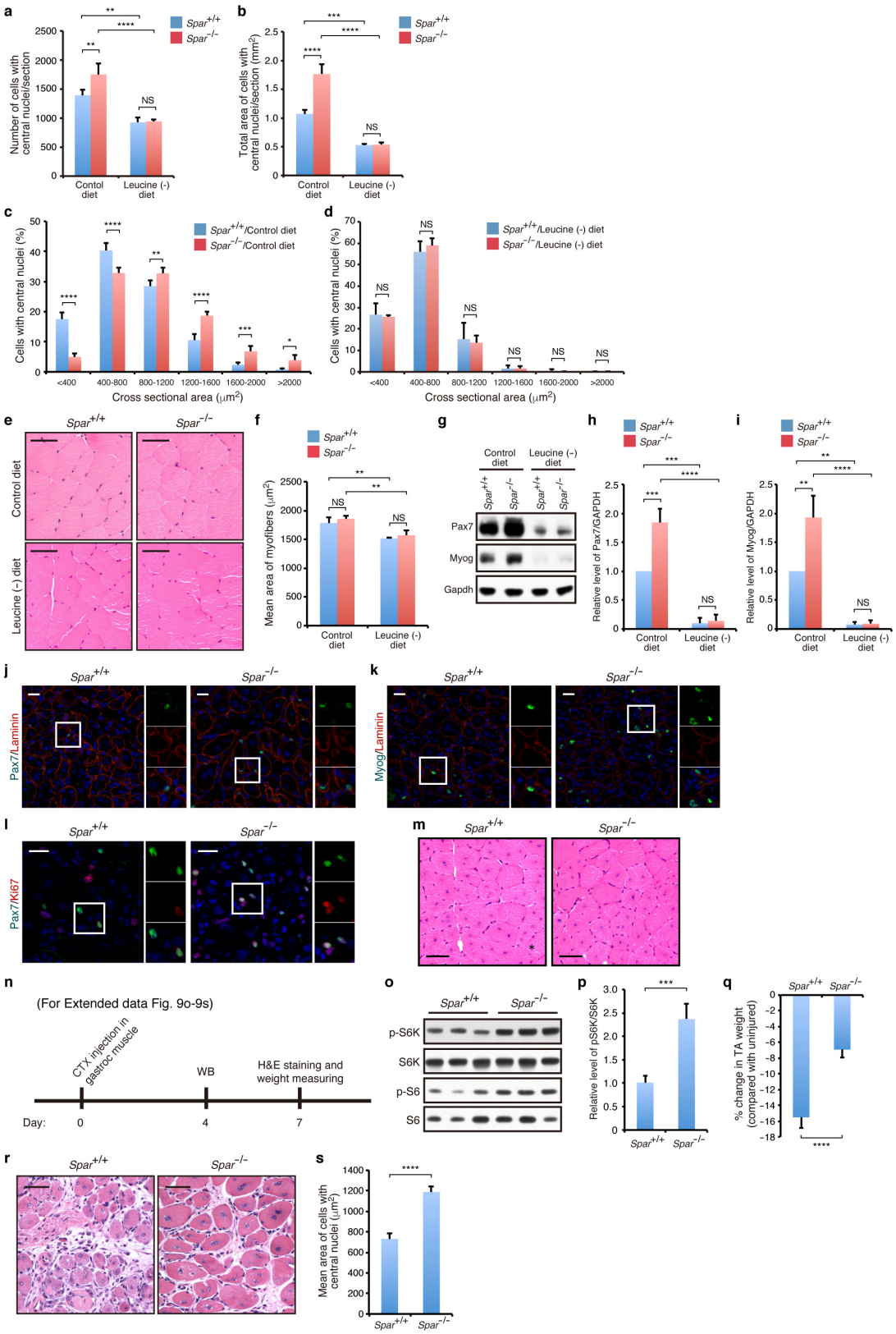

Extended Data Figure 9 | See next page for caption.

Extended Data Figure 9 | Characterization of enhanced regeneration in Spar-deficient tibialis anterior muscle. a, **b**, The number of regenerating myofibres with central nuclei (**a**), and total area of regenerating myofibres with central nuclei (**b**) in regenerating tibialis anterior muscles 7 days after CTX administration in $Spar^{+/+}$ and $Spar^{-/-}$ mice on control diet or leucine-free diet. Data shown as mean ± s.d. ($n = 5$ for control diet, $n = 3$ for leucine-free diet). **c**, **d**, Percentage of myofibres with central nuclei from **a** and **b** analysed according to cell size. Comparisons for $Spar^{+/+}$ and $Spar^{-/-}$ mice on control diet (**c**) and leucine-free diet (**d**) are shown. Data shown as mean ± s.d. ($n = 5$ for control diet, $n = 3$ for leucine-free diet). **e**, **f**, H&E staining of uninjured lateral control tibialis anterior muscle from $Spar^{+/+}$ and $Spar^{-/-}$ mice. Representative images (from at least 10 fields of view per mouse) (**e**), and mean area of myofibres (**f**). Data shown as mean ± s.d. ($n = 3$). Scale bar, 50 μm. **g**–**i**, Immunoblot analysis of Pax7 and Myog in injured tibialis anterior muscle lysates 4 days after CTX administration, from $Spar^{+/+}$ and $Spar^{-/-}$ mice on control or leucine-free diet (**g**), and quantitative analysis of relative level of Pax7 (**h**) and Myogenin (**i**) normalized to Gapdh level. Data shown as mean ± s.d. ($n = 3$). **j**–**l**, Immunofluorescence analysis for Pax7 and laminin (**j**), Myog and laminin (**k**) and Pax7 and Ki67 (**l**) in regenerating tibialis anterior muscle from $Spar^{+/+}$ and $Spar^{-/-}$ mice 4 days after CTX administration. Representative images (from at least six fields of view per mouse) are shown, and the quantification is shown in Fig. 4i, j ($n = 3$). Scale bar, 20 μm. **m**, H&E staining of regenerating tibialis anterior muscle from $Spar^{+/+}$ and $Spar^{-/-}$ mice 14 days after CTX administration. Representative images (from at least 10 fields of view per mouse) are shown, and percentage of mature cells with peripheral nuclei was quantified in Fig. 4k ($n = 3$). Scale bar, 50 μm. **n**, A schematic outlining the experimental timeline to study regeneration of gastrocnemius muscle. **o**, **p**, Phosphorylation status of S6K1 and S6 in regenerating gastrocnemius muscle from $Spar^{+/+}$ and $Spar^{-/-}$ mice 4 days after injury (**o**), and quantitative analysis of relative level of phospho-S6K/total-S6K (**p**). Data shown as mean ± s.d. ($n = 3$). **q**, Per cent change in weight of regenerating gastrocnemius muscle compared with that of uninjured control lateral muscle. Muscles were removed 7 days after CTX administration. Data shown as mean ± s.d. ($n = 4$). **r**, **s**, H&E staining of regenerating gastrocnemius muscle from $Spar^{+/+}$ and $Spar^{-/-}$ mice 7 days after CTX administration. Representative images (from at least five fields of view per mouse) (**r**), and mean area of cells with central nuclei (**s**). Data shown as mean ± s.d. ($n = 4$). Scale bar, 50 μm. $^{*}P < 0.05$, $^{**}P < 0.01$, $^{***}P < 0.001$, $^{****}P < 0.0001$; Student's *t*-test (**p**, **q**, **s**) or two-way ANOVA followed by Tukey's test (**a**–**d**, **f**, **h**, **i**). For gel source images, see Supplementary Fig. 1.

Extended Data Table 1 | The LINC00961-encoded polypeptide interactome identified by mass spectrometric analyses using anti-Flag immunoprecipitates from HEK293T cells expressing Flag KI1

		Identified peptide number	
Gene Symbol	Description	Mock	SPAR
JUP	junction plakoglobin	0	14
ATP6V0A2	**ATPase, H+ transporting, lysosomal V0 subunit a2**	**0**	**9**
STT3B	STT3, subunit of the oligosaccharyltransferase complex, homolog B (S. cerevisiae)	0	9
ATP6V0A1	**ATPase, H+ transporting, lysosomal V0 subunit a1**	**0**	**7**
KRT80	keratin 80	0	7
FAF2	Fas associated factor family member 2	0	6
DSC1	desmocollin 1	0	6
NPLOC4	nuclear protein localization 4 homolog (S. cerevisiae)	0	6
MYO6	myosin VI	0	5
BLMH	bleomycin hydrolase	0	5
FKBP8	FK506 binding protein 8, 38kDa	0	5
TGM3	transglutaminase 3 (E polypeptide, protein-glutamine-gamma-glutamyltransferase)	0	5
SBSN	suprabasin	0	5
PIGT	phosphatidylinositol glycan anchor biosynthesis, class T	0	4
DNAJC16	DnaJ (Hsp40) homolog, subfamily C, member 16	0	4
FLG	filaggrin	0	4
SEC22B	SEC22 vesicle trafficking protein homolog B (S. cerevisiae)	0	4
TXN	thioredoxin	0	4
ANKRD13A	ankyrin repeat domain 13A	0	4
POF1B	premature ovarian failure, 1B	0	4
ATP6V0D1	**ATPase, H+ transporting, lysosomal 38kDa, V0 subunit d1**	**0**	**3**
ATP6AP2	**ATPase, H+ transporting, lysosomal accessory protein 2**	**0**	**3**
TRAFD1	TRAF-type zinc finger domain containing 1	0	3
RTN3	reticulon 3	0	3
EMD	emerin	0	3
SCAMP3	secretory carrier membrane protein 3	0	3
UBQLN2	ubiquilin 2	0	3
PBXIP1	pre-B-cell leukemia homeobox interacting protein 1	0	3
CSTA	cystatin A (stefin A)	0	3
ESYT1	extended synaptotagmin-like protein 1	0	3
KPRP	keratinocyte proline-rich protein	0	3
CAT	catalase	0	3